ISSN 0869-5911, Petrology, 2021, Vol. 29, No. 2, pp. 95–113. © Pleiades Publishing, Ltd., 2021.
Russian Text © The Author(s), 2021, published in Petrologiya, 2021, Vol. 29, No. 2, pp. 115–135.

Evidence of Subduction of the Paleoproterozoic Oceanic Crust in the Khapchan Belt of the Anabar Shield, Siberian Craton

N. I. Gusev[a, *], L. Yu. Sergeeva[a], and S. G. Skublov[b, c]

[a] *Karpinsky Russian Geological Research Institute, St. Petersburg, Russia*

[b] *Institute of Precambrian Geology and Geochronology, Russian Academy of Sciences, St. Petersburg, Russia*

[c] *St. Petersburg Mining University, St. Petersburg, Russia*

**e-mail: nikolay_gusev@vsegei.ru*

Received April 16, 2020; revised June 19, 2020; accepted October 7, 2020

Abstract—Granulite complex on the left side of the Bol. Kuonamka River, below the mouth of the Khapchan River, is composed of melanocratic and mesocratic orthopyroxene–clinopyroxene crystalline schists and leucocratic orthopyroxene and orthopyroxene–clinopyroxene plagiogneisses. The granulites formed after mafic to felsic volcanoplutonic rocks with rare sedimentary interlayers. In terms of chemical composition, the mafic and ultramafic rocks correspond to pyroxenites, gabbronorites, and gabbro-diorites of the tholeiite series. The plagioschists and plagiogneisses were formed after rocks similar to diorites, tonalities, and trondhjemites or their volcanic analogs, and are distinguished by increased contents of Ba, Zr, Y, REE, Nb, and Ta. The concordant U-Pb age of zircon from the diorite protolith of orthopyroxene–clinopyroxene plagioschists is 2095 ± 10 Ma. The Lu-Hf isotopic composition of the zircon (ε_{Hf} (T) = 6.5–12, T_{Hf}(DM) = 1.98–2.22 Ga) indicates the correspondence of its source to the Paleoproterozoic depleted mantle. Two-pyroxene plagiogneisses with a concordant U-Pb zircon age of 2030 ± 17 Ma were formed after tonalites of the calc-alkaline series. They are characterized by well-pronounced negative Ti, Nb, Ta, P anomalies characteristic of subduction magmatism. All studied rocks of the Khapchan Belt have positive ε_{Nd}(T) values from +2.3 to +4.2 and are interpreted as a juvenile suprasubduction complex. It is assumed that the subduction of oceanic crust of this age is associated with the formation of eclogitic diamond, which was noted earlier and widespread in placer deposits in the northeastern Siberian platform.

Keyword: Anabar Shield, Khapchan Belt, Paleoproterozoic, depleted mantle, granulites, suprasubduction complex, zircon, U-Pb age SHRIMP-II, Sm-Nd and Lu-Hf systematics

DOI: 10.1134/S0869591121020041

INTRODUCTION

The Siberian Craton is the largest Precambrian continent in northern Asia. Its basement is made up of a Paleoproterozoic collage of Archean high-grade metamorphosed terranes (Rosen et al., 1994; Griffin et al., 1999; Shatsky et al., 2018). The basement is overlain by Mesoproterozoic–Early Cretaceous sedimentary cover up to 8 km thick, which includes Mesozoic flood basalts (traps). The craton basement is subdivided into Magan (Tungusskaya), Anabar, and Olenek composite terranes (Fig. 1a), which consist of heterogeneous blocks that were amalgamated into a single structure at 2.1–1.8 Ga (Rosen et al., 1994; Griffin et al., 1999). Accretion of the terranes was accompanied by widespread collisional granulite metamorphism, and syncollisional and post-collisional granite magmatism (Rosen et al., 1994).

The Anabar shield is a salient of deeply eroded craton basement over 62 thou. km^2 in area, most part of which is made up of granulite-facies rocks (Fig. 1b). It exposes the terranes of three tectonic provinces: Magan tonalite–trondhjemite–gneiss one in the west, Anabar granulite–orthogneiss one in the central part, and Khapchan granulite–paragneiss one in the east (Rosen and Turkina, 2007). The boundaries of the terranes (granulite blocks) are accompanied by shear zones with the wide manifestation of cataclasis, diaphthoresis, and metasomatism. The terranes are separated by suture zones: Kotuikan–Monkholin suture in the west and Saltakh-Billyakh suture in the east.

The Kotuikan–Monkholin suture is 10–30 km wide and traced for 1300 km to the south and southeast according to geophysical data (Rosen et al., 1994; Griffin et al., 1999). Along this suture, the Daldyn terrane of the Anabar Province is thrust over the Il'in block of the Magan Province. The structure of the zone is determined by the collisional blastomylonite macromelange with widespread syntectonic migmatites, autochthonous and vein granites (Rosen et al., 2005). The peculiar features of the Kotuikan–Monk-

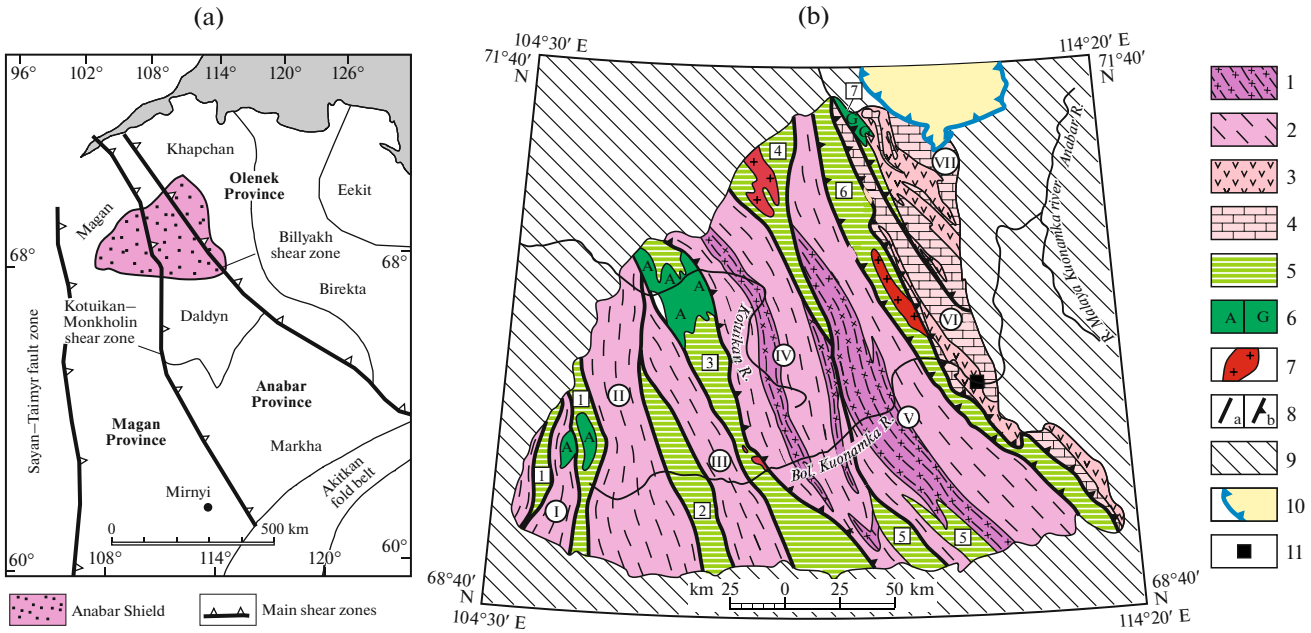

Fig. 1. Tectonic schemes of the (a) northern Siberian Craton after (Rosen et al., 1994; Griffin et al., 1999) and (b) Anabar shield. (1, 2) Archean granulite blocks, associations: (1) metamafic–plagiogneiss (Daldyn Group), (2) plagiogneiss (Upper Anabar Group); (3, 4) Paleoproterozoic granulitic Khapchan Belt, associations: (3) metavolcanogenic; (4) metacarbonate–paragneiss (Khapchan Group); (5) shear zone (tectonite–granite–migmatite association); (6, 7) intrusive rocks, associations: (6A) anorthosite, (6G) gabbrodiorite; (7) granite; (8) main faults: (a) steep; (b) overthrusts; (9) platform cover; (10) Popigai astrobleme; (11) Khapchan site. Granulite blocks (roman numerals in circles): (I) Western, (II) Upper Kuonamka, (III) Il'inskaya, (IV) Daldyn, (V) Dzhelinda, (VI) Khapchan, (VII) Popigai. Shear zones (numerals in boxes): (1) Churbukulakh, (2) Lamui, (3) Kotuikan–Monkholin, (4) Chengelekh; (5) Kharap, (6) Billyakh, (7) Saltakh.

holin zone are large sanukitoid and anorthosite massifs.

The Billyakh suture at a width of 10–20 km is traced for 1500 km to the southeast (Griffin et al., 1999). The structural plan of the Billyakh suture zone is defined by a system of closely spaced and intersecting faults, which bracket blocks and nappes of variably reworked rocks of contacting terranes (Smelov et al., 2012). Blastomylonite and cataclasite zones tracing the faults have reverse fault and updip–strike-slip fault kinematics (Luts and Oxman, 1990). Within the Billyakh structure, the Archean granulites of the Dzhelindinkoi block are in contact with the granulites of the Khapchan fold belt (Rosen et al., 2005).

It is suggested that the basement of the Khapchan belt is made up of granite–greenstone domains of the Birekta terrane, which belongs to the Olenek province (Rosen et al., 2005). The granite–greenstone basement of the Birekta terrane is overlain by the Khapchan metacarbonate–metagraywacke sedimentogenic belt with the age of detrital zircon no older than 2.4 Ga and granulite metamorphism at 1.97 Ga (Rosen et al., 2005). The basement of the sedimentation basin was thought to consist of the Archean granulites of the Daldyn and Upper Anabar groups (Condie et al., 1991). Based on later data on the Paleoproterozoic Nd model age of the granulites of the Khapchan Group, it was concluded that the Khapchan Group was accumulated on a passive margin of the Birekta granite–greenstone terrane (Rosen et al., 2006).

The Khapchan belt includes two granulite-facies rock complexes. The lower complex is represented by mesocratic and leucocratic two-pyroxene and orthopyroxene gneisses that compose layers and units of different thickness. Transitions between them could be both sharp and gradual. This complex also comprises subordinate amounts of melanocratic two-pyroxene and amphibole–two pyroxene crystalline schists in form of conformable lenticular layers and units from a few cm to 300 m thick. The lower complex was usually ascribed to the Archean Upper Anabar Group (Lopatin and Tabunov, 1969).

The upper complex belongs to the Khapchan Group and consists of metasedimentary rocks: garnet and sillimanite gneisses, marbles, calciphyres, and pyroxene–scapolite rocks, the protoliths of which were formed in the Khapchan sedimentary basin (Zlobin et al., 2002). The metasedimentary rocks of the Khapchan Group show thin rhythmic layering. Geochemical features of paragneisses of the Khapchan Group indicate that their protoliths were graywackes, which were similar to those accumulated in the Paleozoic on active or passive continental margins (Condie et al., 1991; Zlobin et al., 2002).

The Khapchan Belt comprises the Anabar diamond region of Yakutia with rich diamond placers, the primary sources of which are not clear yet (Kargin et al., 2017). The placers in the Khapchan zone, as most placers of the northeastern Yakutian province, are dominated (85%) by eclogitic diamonds (Shatsky et al., 2016). Isotope-geochemical data on diamondiferous eclogites show that the eclogites were formed after oceanic crust, which suggests the manifestation of subduction processes on the northeastern Siberian Craton and the presence of subduction component in diamond-bearing mantle (Sun et al., 2020; Kostrovitsky et al., 2016; Shatsky et al., 2016; Zedgenizov et al., 2016).

The age and primary composition of granulites lying below the sedimentogenic section have remained unclear yet. The aim of this study was to determine the composition, age, and geodynamic formation settings of rocks that underlie the metasedimentary rocks of the Khapchan Group and were previously ascribed to the Archean Upper Anabar Group.

GEOLOGY

The studied area is located in the eastern margin of the Anabar shield, being restricted to the emptying of the Khapchan River into the Bol. Kuonamka River (Fig. 2). In this area, the basement crystalline rocks are subsided beneath the Early Riphean cover sediments of the Siberian Platform: the Labaztakh red terrigenous and Kotuikan dolomitic formation. The left bank of the Bol. Kuonamka River recovers the predominant mesocratic plagioschists, which contain bands of mafic crystalline schists in variable proportions (Figs. 3a, 3b) varying in thickness from a few centimeters to 3–5 m. The rocks show wavy metamorphic banding dipping to the northeast at 70°–80°.

A unit of predominant mafic crystalline schists no less than 425 m thick is distinguished at the base of the left bank of the Bol. Kuonamka River. It is overlain by the unit of predominant mesocratic plagioschists 1270 m thick with subordinate intercalations of gneisses and mafic rocks. The upper part of the slope comprises a lenticular band of orthopyroxene and two-pyroxene plagiogneisses with the maximum width of 600 m. Eastward, an unexposed interval separates them from 400–1200 m garnet and garnet–pyroxene gneisses of the Khapchan Group (Fig. 3f). All rocks are deformed into folds and intensely migmatized (Figs. 3c, 3e) and frequently are represented by metatexites and diatexites, the distinctive features of which are considered in (Sawyer, 2008). The granitoid leucosome of the migmatites lies conformably with banding or forms irregularly shaped discordant bodies of variable thickness. The garnet gneisses are overlain by brownish-brown limonitized quartz gravelstones of the Early Riphean Labaztakh Formation. An isolated exposure (200 × 500 m in size) of ultramafic and mafic crystalline schists (Fig. 3d) with alternation of ultramafic and plagioclase varieties is observed among red sandstones downstream, on the right bank of the Bol. Kuonamka River, 4.5 km from the Khapchan River mouth. Rocks visually unaffected by migmatization and migmatite leucosome were collected for geochemical study.

METHODS

Concentrations of major and trace elements were determined by XRF and ICP methods at the Laboratory of the Karpinsky Russian Geological Research Institute, St. Petersburg. Ferric and ferrous iron was determined by titration. The uncertainties of XRF analysis were no greater than 5 rel %. The detection limits of trace elements were from 0.005 to 0.1 ppm, and the analyses were accurate to 2–7 rel %.

The U-Pb zircon dating was conducted on a SHRIMP-II probe at the Center for Isotope Studies (CIS) of the Karpinsky Russian Geological Research Institute (VSEGEI) (St. Petersburg, analyst P.A. L'vov) following conventional technique (Williams, 1998). Areas (spots) for dating were selected using optical (in transmitted and reflected light) and cathodoluminescence (CL) images, which showed the inner structure and zoning of the zircon. The intensity of the primary molecular oxygen beam was 4 nA, the diameter of the spot (crater) was 25 μm, and its depth was 2 μm. The raw data were processed with the SQUID software (Ludwig, 2000). The U-Pb ratios were normalized to 0.0668, a value for the TEMORA zircon standard dated at 416.75 Ma (Black et al., 2003). The inaccuracies of individual analyses (ratios and ages) are reported at 1σ level, and the inaccuracies of the calculated values of concordant ages and intercepts with a concordia are presented at 2σ level. The plots were constructed using the ISOPLOT/EX program (Ludwig, 1999).

The Lu-Hf isotope composition of zircon was analyzed by LA-ICP-MS using a COMPex-102 193-nm ArF laser equipped with a DUV-193 ablation system and a ThermoFinnigan Neptune multicollector mass spectrometer in inductively coupled plasma at the Center for Isotope Studies of the Karpinsky Institute (analyst I.N. Kapitonov), using technique described in (Griffin et al., 2000). The configuration of the collectors enabled a simultaneous registration of the ^{172}Yb, ^{174}Yb, ^{175}Lu, ^{176}Hf, ^{177}Hf, ^{178}Hf, and ^{179}Hf isotopes. Correction for mass discrimination was made using a single normalizing ratio (^{178}Hf/^{177}Hf). The corrected ^{176}Hf value was obtained by subtracting ^{176}Yb and ^{176}Lu (the measured values were interference-free ^{172}Yb and ^{175}Lu) (Kapitonov et al., 2007). The isotope composition was analyzed at the spots of U-Pb dating, but the crater was ~50 μm across and 20–40 μm deep. At the time of measurements, the ^{176}Hf/^{177}Hf ratios of the zircon standards were 0.282701 ± 35 (TEMORA, $n = 6$), 0.282497 ± 27 (Mud Tank, $n = 5$) and 0.282009 ± 23 (GJ-1, $n = 7$). These values agree with the pub-

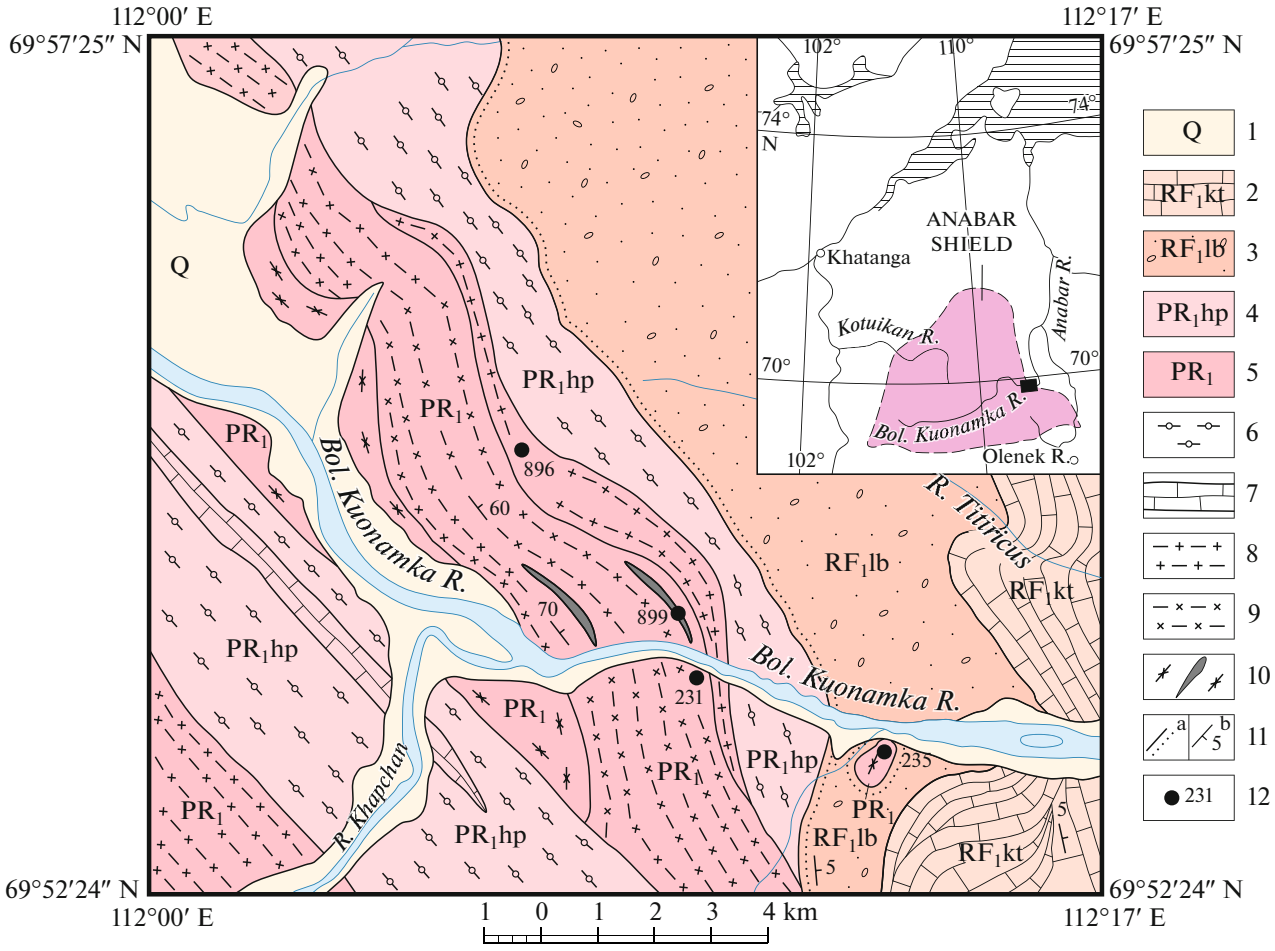

Fig. 2. Geological scheme of the Khapchan site. Filled box shows the position of the Khapchan site in inset. (1) loose Quaternary sediments; (2) Kotuikan Formation (RF_1kt): dolomites, sandy dolomites; (3) Labaztakh Formation (RF_1lb): red sandstones, gravelstones, conglomerates; (4) Khapchan Group (PR_1hp): garnet, biotite–garnet, garnet–pyroxene, and sillimanite–garnet paragneisses, marbles, calciphyres, pyroxene–scapolite rocks; (5) Paleoproterozoic undivided rocks (PR_1): orthopyroxene and two-pyroxene plagiogneisses, mesocratic and mafic crystalline schists previously ascribed to the Archean Upper Anabar Group; (6) garnet-bearing gneisses; (7) carbonate and metacarbonate rocks; (8) leucocratic pyroxene orthogneisses; (9) mesocratic gneisses and plagioschists; (10) mafic crystalline schists; (11) unconformable boundaries (a), dip and strike (b); (12) geochronological sampling localities and their numbers.

lished ones: 0.282680 ± 24 for TEMORA (Woodhead et al., 2004), 0.282504 ± 44 for Mud Tank (Woodhead and Hergt, 2005), and 0.282015 ± 19 for GJ-1 – (Elhlou et al., 2006). The data were processed using a decay constant $^{176}Lu = 1.865 \times 10^{-11}$ yr^{-1} (Scherer et al., 2001). The $\varepsilon_{Hf}(T)$ values were calculated using the chondrite values: $^{176}Lu/^{177}Hf = 0.0332$ and $^{176}Hf/^{177}Hf = 0.282772$ (Blichert-Toft and Albarede, 1997). The Hf-model age was determined relative to the depleted mantle (DM) with $^{176}Lu/^{177}Hf = 0.0384$ and $^{176}Hf/^{177}Hf = 0.28325$ (Chauvel and Blichert-Toft, 2001). Because the zircon model age ($T_{Hf}(DM)$ corresponds to the minimum age of the source of the melt from which this zircon crystallized, we have also calculated the more valid two-stage age T^{C}_{Hf}, which was obtained by projecting the initial $^{176}Hf/^{177}Hf$ ratio of zircon onto the line of the depleted mantle with the use of the average crustal value of $^{176}Lu/^{177}Hf = 0.015$ (Griffin et al., 2000).

The Sm-Nd isotope composition was studied using conventional procedures for separation of elements (*Izotopnaya geologiya ...*, 2017, p. 128). The isotope measurements were conducted on a ThermoFinnigan MAT TRITON mass spectrometer at the Center for Isotope Studies at the Karpinsky Institute (analyst E.S. Bogomolov). The measured $^{143}Nd/^{144}Nd$ ratios were corrected for isotope fractionation relative to $^{146}Nd/^{144}Nd = 0.7219$ and adjusted to $^{143}Nd/^{144}Nd = 0.512117$ in the JNdi-1 standard. The total blanks during the measurements were 0.03–0.2 ng for Sm and 0.1–0.5 ng for Nd. The Sm and Nd concentrations were measured accurate to ±0.5% (2σ), and $^{147}Sm/^{144}Nd$ and $^{143}Nd/^{144}Nd$ ratios, to ±0.5 and

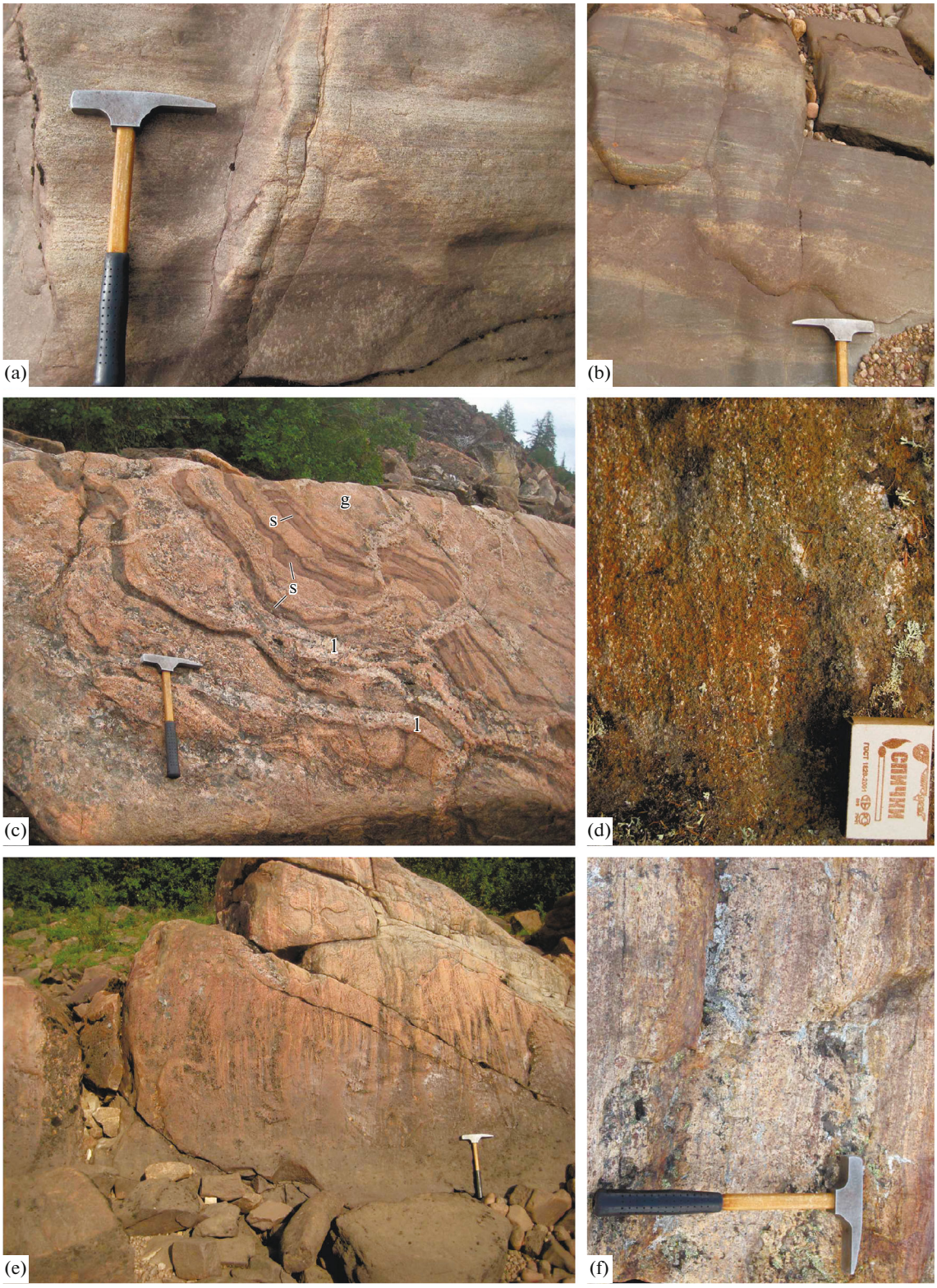

Fig. 3. Major types of metamorphic rocks of the Khapchan site: (a) mesocratic two-pyroxene plagioschists; (b) lenticular alternation of mafic and mesocratic crystalline schists; (c) schlieren diatexites: (g) leucosome (sample 900); (s) melanosome, (l) plagiogranite leucosome of superimposed migmatites (sample 900-1); (d) lenticular-banded two-pyroxene crystalline schists (sample 236); (e) migmatized orthopyroxene plagiogneisses (sample 561); (f) garnet gneisses of the Khapchan Group (sample 49-4).

±0.005%, respectively. The $\varepsilon_{Nd}(T)$ were calculated using the following present-day isotope ratios for chondrite uniform reservoir (CHUR): $^{147}Sm/^{144}Nd$ = 0.1967 and $^{143}Nd/^{144}Nd$ = 0.512638 (Jacobsen and Wasserburg, 1984). A one-stage model age ($T_{Nd}(DM)$ was calculated relative to depleted mantle (DM) with $^{147}Sm/^{144}Nd$ = 0.2136 and $^{143}Nd/^{144}Nd$ = 0.513151 (Goldstein and Jacobsen, 1988). Mineral abbreviations are given according to (Whitney and Evans, 2010).

RESULTS

Geological-petrographic characteristics. Granulites of the Khapchan site are subdivided into four rock groups: two-pyroxene crystalline schists (Figs. 3a, 3b, 3d), two-pyroxene and orthopyroxene gneisses (Figs. 3c, 3e), and garnet gneisses (Fig. 3f).

The two-pyroxene (Cpx–Opx) crystalline schists occur mainly near the Bol. Kuonamka River bed and form an isolated exposure among Riphean red rocks in its right bank. The exposures are represented by lenticular banded ultramafic and mafic varieties (Fig. 3d) related by gradual transitions. In this exposure (Fig. 3d), the ultramafic crystalline schists (sample 235) containing (in vol %) *Opx* 45, *Cpx* 30, *Hbl* 20, *Srp* 2, *Chr* 3 gradually pass into mafic crystalline schists (sample 236) with composition (in vol %): *Pl* (An_{42}) 55, *Opx* 25, *Cpx* 5, *Hbl* 14, *Mag* 1. The two-pyroxene crystalline schists in thick mafic lenses among gneisses (sample 899) are made up of (in vol %) antiperthitic *Pl* (An_{40}) 35–40, *Cpx* 27, *Opx* 23, *Qz* 5–10, *Mag* 5 and single flakes of dark brown *Bt*. The most abundant mesocratic two-pyroxene plagioschists (sample 231) have the following mineral composition (in vol %): *Pl* (An_{30}) 65, *Cpx* 20, *Opx* 10, *Mag* 2, *Ap* 1, *Bt* 1. They are alternated with *two-pyroxene gneisses* represented by ortho- or clinopyroxene-dominated varieties. The orthopyroxene-dominated two-pyroxene gneisses (sample 565) contain (in vol %): *Pl* (An_{33}) 67, *Qz* 13–14, *Opx* 11–12, *Cpx* 2–3, and *Ap* 0.5. The clinopyroxene-dominated two-pyroxene varieties (sample 896) differ in more calcic plagioclase at high quartz content (in vol %): *Pl* (An_{42}) 50, *Qz* 25–30, *Cpx* 10, *Opx* 1–2, *Mag* 2, and *Ttn* 1.

The orthopyroxene gneisses are represented by rocks with approximately equal contents of *Qz* and *Opx* (samples 564, 565A, composition in vol %): *Pl* (An_{30}) 47–63, *Qz* 17–25, *Opx* 16–24, *Mag* 3–4), and more leucocratic varieties (samples 561, 897, 900) with composition (in vol %): anthiperthitic *Pl* (An_{17-21}) 60, *Qz* 25–30, *Opx* 6–10, *Bt* 0–3, *Mag* 2, and single grains of *Ap* and *Zrn*. The plagiogranite leucosome of vein migmatites (sample 900-1) consists mainly of (in vol %): *Pl* (An_{30}) 70, *Qz* 20–25, and mafic mineral represented by *Hbl* 5 developed after *Opx* 1.

The garnet gneisses of the Khapchan Group (samples 49-4, 52-2) contain (in vol %): predominant antiperthitic *Pl* (An_{50}) 30–40, *Qz* 23–24, *Grt* 15–25, *Or* 12–15, *Bt* 3–5, and single *Mag, Ap,* and *Zrn*.

Geochemistry of the rocks (Table 1) is analyzed using all major rock components (Fig. 4a) and based on diagram for immobile high field strength elements Zr/Ti–Nb/Y (Fig. 4b), equivalent TAS diagram (Pearce, 1996), and Th–Co diagram (Fig. 4c) that is similar to the K_2O–SiO_2 diagram (Hastie et al., 2007). Felsic rocks were plotted in the normative Ab–An–Or classification diagram (Fig. 4d) (O'Connor, 1965).

The two-pyroxene crystalline schists correspond in chemical composition (Table 1, Fig. 4a) to tholeiites (samples 235, 236), basaltic andesite (sample 899), and latite (sample 231). Ultramafic and mafic rocks and crystalline schists (samples 235, 236 in Fig. 4a) corresponding to pyroxenite and gabbronorite (Mg#[1] = 78.9–65.4) have the highest contents of Cr, Ni, and Pb. They are depleted in REE (ΣREE = 19.7–23.4 ppm). Metapyroxenites are characterized (Figs. 5a, 5b) by a negative slope of REE distribution pattern $(La/Yb)_N$ = 0.7, Eu-minimum (Eu/Eu* = 0.51) and negative Sr anomaly, which is related to the plagioclase fractionation and its accumulation in metagabbronorites $(La/Yb)_N$ = 1.7, Eu/Eu* = 1.54, Sr/Y = 33.1). The mafic crystalline schist (sample 899) is petrochemically equivalent to basaltic andesite or gabbrodiorite (Mg# = 46), but differs in the positive Ba anomaly, negative Pb, Sr, Eu, and Ti anomalies, weak REE fractionation $(La/Yb)_N$ = 1.82), and well expressed Eu-minimum (Eu/Eu* = 0.64). The mesocratic two-pyroxene plagioschists (sample 231, Mg# = 40) are metaluminous ASI[2] = 0.82. Petrochemically, they correspond to latite/monzonite, but moderately alkaline affinity is not confirmed by the trace-element abundance (Figs. 4b, 4c). Therefore, further, these rocks are termed as metadiorites. Spidergrams (Figs. 5a, 5b) show a positive Ba anomaly and negative anomalies of Th, Pb, Sr, and Ti, but Ta and Nb anomalies are absent. REE patterns are weakly fractionated $(La/Yb)_N$ = 3.1) and have Eu-minimum (Eu/Eu* = 0.89).

The two-pyroxene gneisses (samples 565, 896) chemically (Figs. 4a, 4d) correspond to dacite/tonalite (Mg# = 33–44). The rocks are metaluminous (ASI = 0.72–0.93), while orthopyroxene-dominated varieties (sample 565) have negative Th, Pb, and Sr (Figs. 5c, 5d) anomalies but lack negative Ta and Nb anomalies. The REE distribution is relatively weakly fractionated $(La/Yb)_N$ = 4, shows a positive Eu anomaly (Eu/Eu* = 1.22), and Sr/Y = 8.3. The clinopyroxene-dominated varieties (sample 896) have more contrasting trace-element distribution with sharply expressed Ba, U, Pb,

[1] Mg# = Mg/(Mg + Fe), in mol %.

[2] ASI (aluminum saturation index) = $Al_2O_3/(CaO + Na_2O + K_2O)$, in mol %.

Table 1. Contents of major (wt %) and trace (ppm) elements in granulites

Components	235*	236	899	231	565	564	561	565A	897	896	900	49-4	52-2	900-1
	1	2	3	4	5	6	7	8	9	10	11	12	13	14
SiO_2	51.7	50.8	51.7	54.7	60.4	65.7	70.0	63.0	72.0	67.6	75.0	62.7	61.5	67.4
TiO_2	0.36	0.34	1.11	1.4	1.13	0.47	0.38	0.84	0.42	0.21	0.26	0.8	1.06	0.09
Al_2O_3	3.27	18.2	8.84	16.4	16.2	11.6	15.2	15.2	13.7	14.9	13.3	17.2	18.1	18.8
Fe_2O_3	2.17	1.13	5.63	2.72	2.93	3	1.41	2.13	1.50	1.07	1.58	3.94	3.99	0.57
FeO	8.02	6.45	11.4	7.88	5.87	5.16	2.58	6.02	2.88	2.24	1.52	3.39	3.96	0.86
MnO	0.18	0.13	0.32	0.18	0.15	0.19	0.08	0.13	0.08	0.06	0.05	0.15	0.10	0.02
MgO	20.9	7.91	8.05	3.82	2.35	6.67	1.00	3.10	0.91	1.41	0.30	3.14	2.79	0.67
CaO	11.6	11.1	9.45	5.90	5.14	2.86	2.25	3.90	2.51	8.07	1.88	1.90	1.63	4.20
Na_2O	0.05	2.45	2.22	5.36	4.89	3.62	5.40	4.59	4.88	2.92	4.58	3.55	3.09	5.46
K_2O	0.23	0.28	0.56	0.67	0.26	0.19	1.15	0.50	0.76	0.97	1.03	2.13	2.56	1.06
P_2O_5	0.02	0.02	0.12	0.23	0.22	<0.05	0.1	0.10	0.08	<0.05	<0.05	0.07	0.06	<0.05
L.O.I.	<0.01	0.38	<0.01	0.05	<0.01	<0.01	0.35	<0.01	0.23	0.44	0.19	0.71	0.92	0.79
Total	98.50	99.19	99.40	99.31	99.54	99.46	99.90	99.51	99.95	99.89	99.69	99.68	99.76	99.92
Th	<0.01	<0.01	0.89	0.27	0.42	0.77	0.75	0.41	4.14	4.53	1.22	8.0	0.92	2.22
U	<0.01	<0.01	0.23	0.20	0.25	0.54	0.2	0.19	1.22	1.36	0.32	0.66	0.53	0.36
Rb	<2	2.41	4.37	5.83	<2	<2	7.76	2.27	4.87	12.3	6.31	19.40	23.30	5.66
Ba	<3	82	115	307	162	87.2	293	71.5	110	585	227	667	516	361
Sr	15.4	331	101	134	180	64.7	87.2	126	107	709	171	190	199	406
La	1.19	2.83	9.77	15.1	11.7	13.2	20.2	11.8	30.9	18.9	21.1	47.3	41.9	23.6
Ce	4.33	6.36	25.3	37.9	25.9	29.5	42.6	23.5	69.5	30.9	42.3	86.9	76.6	36.6
Pr	0.85	1.00	3.78	5.57	3.33	3.77	5.30	2.93	9.05	3.39	4.92	9.25	8.05	3.49
Nd	4.66	4.84	20.0	24.0	14.7	15.9	21.8	12.3	38.5	14.2	19.6	34.1	26.9	11.1
Sm	1.60	1.23	4.85	6.13	3.57	4.14	4.69	2.88	8.76	2.29	4.19	5.97	4.54	1.68
Eu	0.26	0.71	1.10	1.74	1.47	1.06	1.46	0.95	1.34	1.06	1.43	1.71	1.50	1.27
Gd	1.54	1.61	5.70	5.84	3.78	5.47	4.82	3.06	9.04	2.15	3.67	6.78	6.08	1.31
Tb	0.30	0.29	1.04	1.04	0.62	0.98	0.75	0.48	1.64	0.31	0.61	1.24	0.95	0.20
Dy	1.88	1.70	6.78	6.87	4.10	6.95	4.65	3.10	9.86	1.65	3.07	9.69	7.45	1.17
Ho	0.42	0.39	1.46	1.35	0.74	1.60	0.97	0.66	2.26	0.40	0.84	2.14	1.37	0.26
Er	1.13	1.02	4.01	4.09	2.51	4.81	2.75	1.98	6.84	1.11	2.49	6.92	4.05	0.81
Tm	0.17	0.14	0.52	0.5	0.34	0.76	0.42	0.29	1.03	0.15	0.37	1	0.67	0.13
Yb	1.24	1.13	3.61	3.26	1.96	5.2	2.77	2.05	5.86	1.26	2.57	6.51	4.05	0.87
Lu	0.16	0.15	0.6	0.54	0.37	0.80	0.41	0.32	0.78	0.21	0.33	0.99	0.59	0.13
Zr	13.9	8.04	114	206	139	170	169	110	284	161	321	186	202	39.2
Hf	0.64	0.42	3.39	5.34	3.74	4.90	5.05	3.10	8.05	4.07	8.26	4.83	5.38	1.10
Ta	<0.1	<0.1	0.49	0.57	0.50	0.52	0.41	0.41	1.87	0.32	0.15	0.85	2.84	0.14
Nb	<0.5	0.50	7.22	12.7	7.25	8.91	10.10	5.94	22.90	5.08	5.95	12.70	27.60	2.75
Y	10.7	10.0	34.4	34.3	21.6	40.8	24.9	17.0	64.0	11.0	22.9	62.0	42.4	6.69
Cr	3000	184	51.3	29.1	14.6	165	1.14	7.06	32.5	44	18.3	139	108	4.51
Ni	358	54.3	33.7	41	18.8	65.9	1.77	25.2	27.8	8.64	12.8	49.9	5.64	<1.0
Co	45.8	35.7	50.3	28.7	19.8	23.1	5.31	26.2	6.19	6.6	2.23	9.33	4.03	0.6
Sc	53.4	35.9	49.9	23.7	16.6	25.2	9.75	17.8	12.9	8.77	7.16	26.8	25.0	0.47
Pb	4.93	5.28	<1.0	1.28	1.21	1.45	3.08	2.55	2.32	12.30	2.31	15.30	15.30	149
Ga	6.28	17.3	14.6	21.4	19.7	12.9	15	15.9	19.3	16.3	18.9	15.5	15.9	18.1
Eu/Eu*	0.51	1.54	0.64	0.89	1.22	0.68	0.94	0.98	0.46	1.46	1.12	0.82	0.87	2.62
$(La/Yb)_N$	0.7	1.7	1.8	3.1	4.0	1.7	4.9	3.9	3.6	10.1	5.5	4.9	7.0	18.3
ΣREE	19.7	23.4	88.5	114	75.1	94.1	114	66.3	195	78.0	108	221	185	82.6

(1–3) ultramafic (sample 235) and mafic (samples 236, 899) two-pyroxene crystalline schists; (4, 5) mesocratic two-pyroxene plagioschists (sample 231) and gneisses (sample 565); (6–9) orthopyroxene plagiogneisses (samples 561, 564, 565A, 897); (10) clinopyroxene plagiogneisses (sample 896), (11) orthopyroxene plagiogneisses of diatexites (sample 900); (12, 13) garnet gneisses of the Khapchan Group (samples 49-4, 52-5); (14) tonalite leucosome of migmatites (sample 900-1).
* Sample numbers.

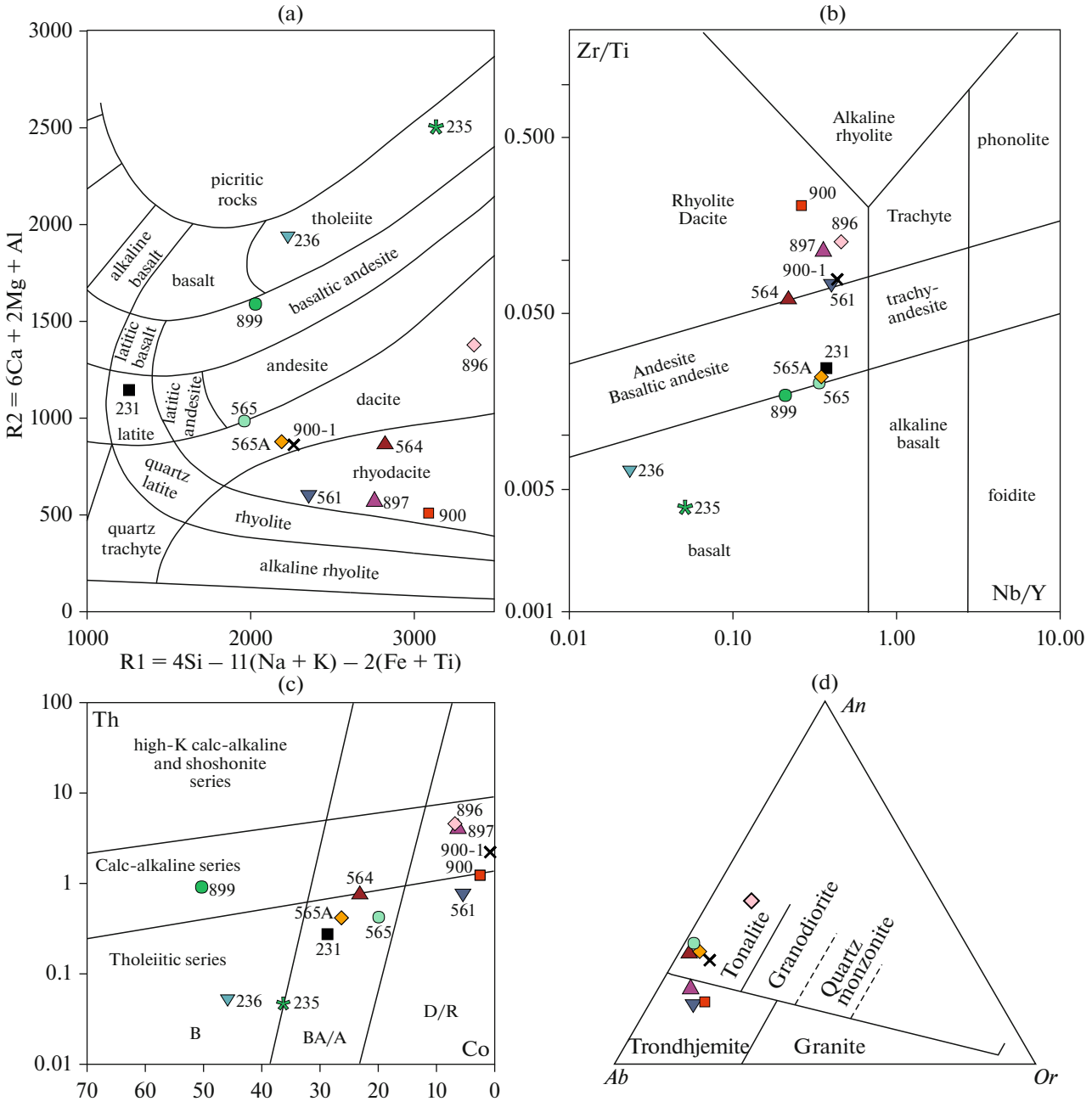

Fig. 4. Geochemical diagrams for granulites of the Khapchan site. (a) after (De la Roche et al., 1980); (b) after (Pearce, 1996); (c) after (Hastie et al., 2007), (d) after (O'Connor, 1965). Sample numbers near data points correspond to those in Table 1. Fields in the diagram: (c): (B) basalts, (BA/A) basaltic andesite/andesite; (D/R) dacite/rhyolite.

Sr, and Zr anomalies, more fractionated REE pattern $(La/Yb)_N$ = 10.1, positive Eu-anomaly (Eu/Eu* = 1.46), and high Sr/Y = 64.5. The rocks show clearly expressed negative Nb, Ta, Ti, and P anomalies.

The orthopyroxene gneisses correspond to dacite/tonalite (samples 564, 565A, 900-1) and rhyodacite/trondhjemite (samples 561, 897, 900) (Figs. 4a, 4d). The rocks are peraluminous (ASI = 1.0–1.1), with Mg# = 41–60 and 15–32 in tonalites and trondhjemite varieties, respectively. Tonalitic granulites (Figs. 5e, 5f, sample 565A) are characterized by poor positive Ba, La, Pb, and Zr anomalies and weakly fractionated REE pattern $(La/Yb)_N$ = 3.9, and lack Eu-minimum (Eu/Eu* = 0.98). Orthopyroxene-rich varieties (sample 564, Mg# = 60) differ in the elevated contents (in ppm) of Cr 165, Ni 65.9, and Zr 170. The spidergrams reveal positive Ba, U, and Zr anomalies, and negative Pb, P, and Ti anomalies. The REE content is low (ΣREE = 94.4 ppm), REE pattern is weakly

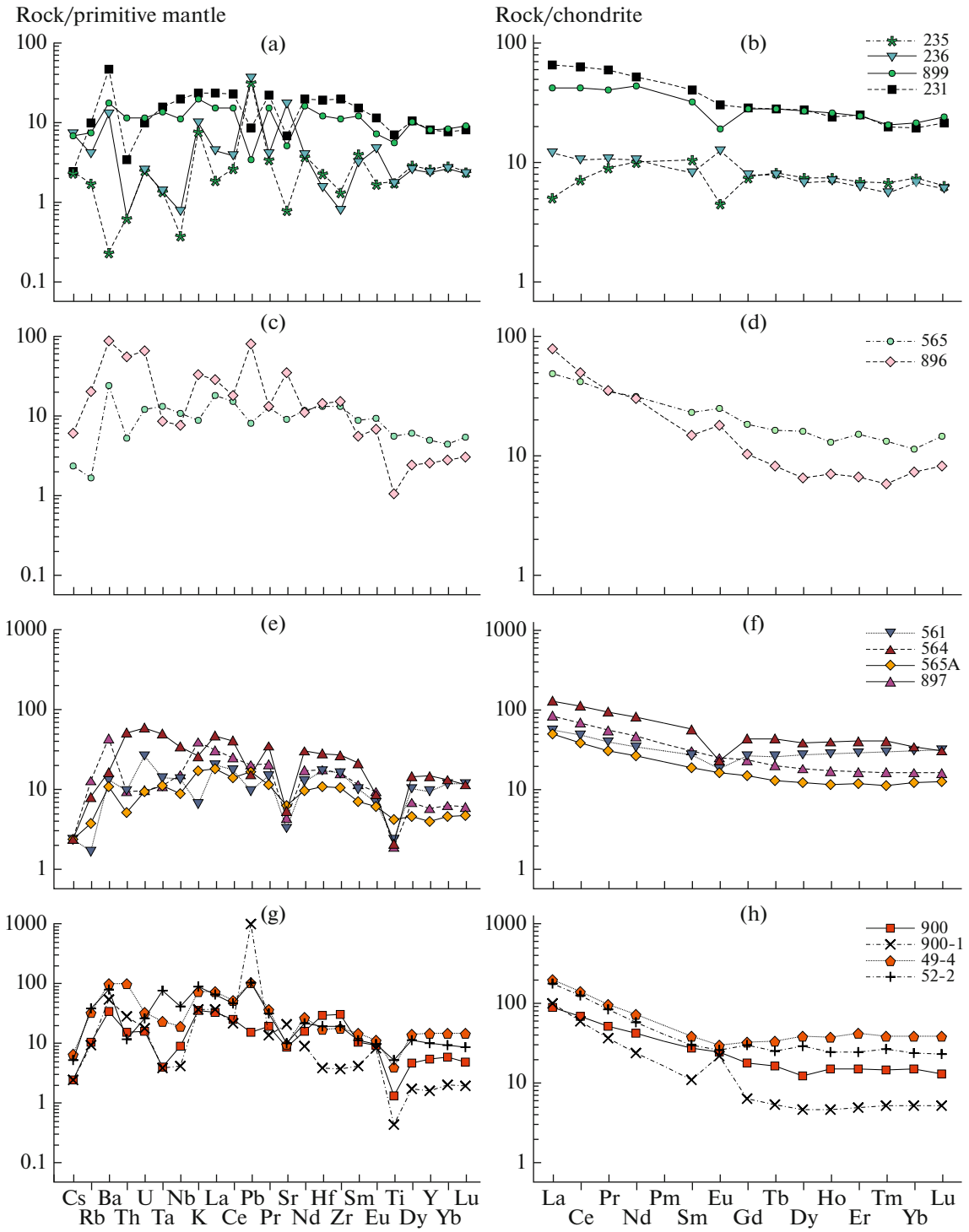

Fig. 5. Multielement diagrams for granulites of the Khapchan site. (a, b) *Cpx–Opx* crystalline schists, (c, d) *Cpx–Opx* gneisses; (e, f) *Opx* gneisses; (g, h) *Opx* leucosome of migmatites and *Gr* gneisses of the Khapchan Group. The contents were normalized to primitive mantle and chondrite after (Sun, McDonough, 1989). Sample numbers correspond to those in Table 1.

fractionated $(La/Yb)_N$ = 1.73, with clear Eu-minimum (Eu/Eu* = 0.68). The leucosome of vein migmatites (Figs. 5g, 5h, sample 900-1) is enriched in Ba, Pb, Sr, Eu, and Zr, and has high Sr/Y = 60.7. The REE pattern is fractionated $(La/Yb)_N$ = 18.3) and exhibits a positive Eu-anomaly (Eu/Eu* = 2.62).

The garnet gneisses of the Khapchan Group differ in the elevated contents (in wt %) of K_2O 2.13–2.56

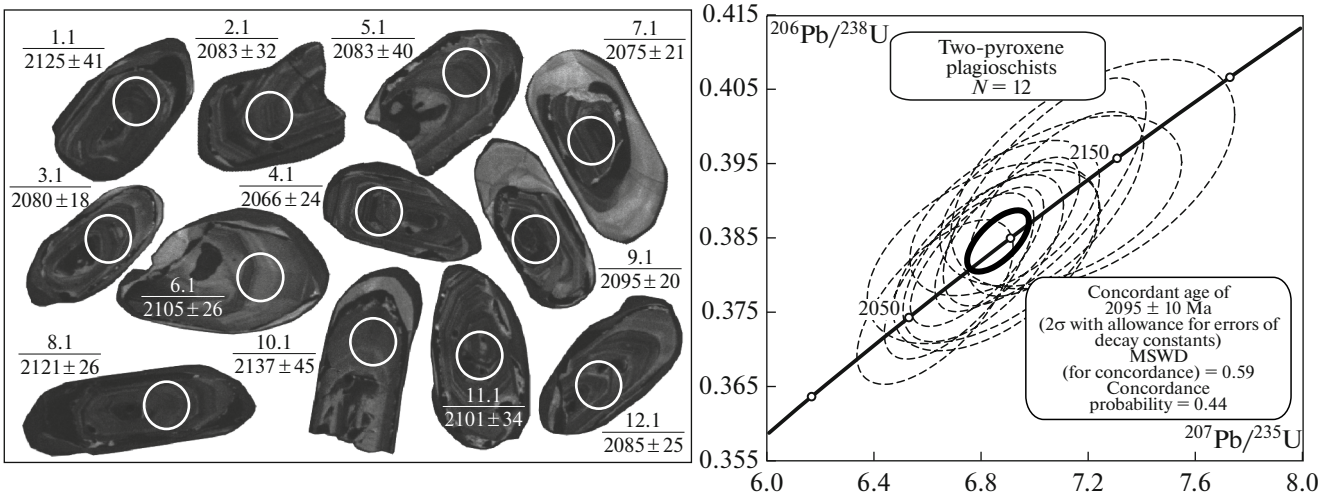

Fig. 6. Cathodoluminescence (CL) images and age of zircon from mesocratic two-pyroxene plagioschists (sample 231). White circles show analytical craters, analysis numbers, in nominators, and $^{207}Pb/^{206}Pb$ age, in denominator. Crater diameter accounts for about 20 μm.

and Al_2O_3 17.2–18.1, and, correspondingly, high ASI = 1.49–1.68. The spidergrams (Figs. 5g, 5h) have positive Ba, Pb, and Nd anomalies and negative P and Ti anomalies. The Th, Nb, and Ta contents display both positive and negative anomalies. They have high REE contents (ΣREE = 185–221 ppm), weakly expressed Eu-minimum (Eu/Eu* = 0.82–0.87), fractionated LREE pattern $(La/Yb)_N$ = 4.9–7, and flat HREE $(Gd/Yb)_N$ = 0.8–1.1.

U-Pb age. Zircon (Table 2) was dated in three samples: (1) mesocratic two-pyroxene plagioschist (sample 231), (2) two-pyroxene plagiogneiss (sample 896), and (3) mafic two-pyroxene crystalline schist (sample 899). Ultramafic two-pyroxene crystalline schists (sample 235) yielded no zircon.

In the **mesocratic plagioschist** (sample 231), zircon is represented by rounded and oval short-prismatic grains (Fig. 6). The grains are colorless, brown and yellowish, transparent and translucent, the length from 100 to 300 μm, with elongation coefficient of 1–2. All grains in CL-images consist of dark cores and shells of variable thickness and tints. The cores show rhythmic and sectorial zoning. Based on 12 analyses, the cores contain (in ppm): U 63–143, Th 15–101, Th/U 0.32–0.73. The concordant age of 2095 ± 10 Ma is considered as the crystallization age of magmatic protolith of the plagioschist.

The two-pyroxene plagiogneiss contains colorless and pink zircon, with cores and overgrowths. The cores in CL-images show rhythmic zoning (Fig. 7), while shells are homogenous and CL-dark. Two cores (an. spots 1.1 and 8.1) contain (in ppm): U 183–187, Th 104–111, Th/U = 0.58–0.61 and have a concordant age of 2121 ± 23 Ma. The rhythmically zoned cores of the second group (six analyses) contain (in ppm) U 110–491, Th 91–189, Th/U = 0.20–0.85 and have an upper intercept age of 2030 ± 17 Ma. Black shells of the zircon (points 5.2 and 6.2 in CL) have (in ppm) U 633–634, Th 134–167, Th/U = 0.22–0.27 and upper intercept age of 1967 ± 18 Ma. Since the two-pyroxene gneiss is metamagmatic rocks (Fig. 11a, sample 896), zircon of magmatic genesis with an age of 2121 ± 23 Ma was likely inherited or entrained, while the age of magmatic protolith of the plagiogneiss corresponds to the age of magmatic zircon of 2030 ± 17 Ma. Taking into account the wide development of migmatites on the Khapchan site, the black shells of the zircon were likely formed during crystallization of an anatectic melt.

Zircon from the **mafic crystalline schist** (Fig. 8) is white, with diamond luster, sometimes with brownish cores and well discernible thin growth boundaries in the central parts of the grains. In CL-images, the grains are dark, with coarse concentric zoning: the core is slightly darker, the middle part is gray, and shell again is almost black. Ten analyses were made in cores and five analyses, in shells. The cores are characterized by the following average contents (in ppm): U 647, Th 196, Th/U = 0.33. The shells contain: U 72, Th 81, Th/U = 0.30. The ages of the cores and shells show no differences. Obtained concordant age is 1964 ± 6 Ma, which is identical to the age of 1967 ± 18 Ma on black shells of zircons from the two-pyroxene gneiss, sample 896. In both cases, zircon likely crystallized from anatectic melt.

Sm-Nd isotope systematics of the rocks was studied in ten samples (Table 3). A low positive value of $\varepsilon_{Nd}(T)$ = +1.1 in the paragneisses of the Khapchan Group suggests a small contribution of Archean terrigenous material in these sediments. All other rocks have higher $\varepsilon_{Nd}(T)$ from +2.3 to +4.2 and plot slightly below the depleted mantle Nd evolution curve (Fig. 9), which

Table 2. Results of U-Pb (SHRIMP-II) zircon analyses

Analysis spots	$^{206}Pb_c$, %	U, ppm	Th, ppm	$\frac{^{232}Th}{^{238}U}$	$^{206}Pb^*$, ppm	$^{206}Pb/^{238}U$ age, Ma	$^{207}Pb/^{206}Pb$ age, Ma	D, %	(1) $^{238}U/^{206}Pb$	±%	(1) $^{207}Pb^*/^{206}Pb^*$	±%	(1) $^{207}Pb^*/^{235}U$	±%	(1) $^{206}Pb^*/^{238}U$	±%	Rho
Sample 231																	
1.1	0.30	96	40	0.43	32.1	2123 ± 22	2125 ± 41	0	2.554	1.2	0.1321	2.3	7.10	2.6	0.3901	1.2	0.454
2.1	0.25	110	40	0.37	36.7	2113 ± 20	2083 ± 32	−1	2.570	1.1	0.1289	1.8	6.89	2.1	0.3878	1.1	0.527
3.1	0.00	143	101	0.73	47.1	2089 ± 19	2080 ± 18	0	2.613	1.0	0.1286	1.0	6.79	1.5	0.3826	1.0	0.715
4.1	0.14	101	41	0.43	32.6	2060 ± 21	2066 ± 24	0	2.651	1.2	0.1277	1.4	6.63	1.8	0.3765	1.2	0.652
5.1	0.58	81	35	0.45	26.9	2091 ± 23	2083 ± 40	0	2.591	1.3	0.1289	2.3	6.81	2.6	0.3831	1.3	0.498
6.1	0.00	63	21	0.34	21.2	2129 ± 29	2105 ± 26	−1	2.556	1.6	0.1305	1.5	7.04	2.2	0.3913	1.6	0.727
7.1	0.00	99	46	0.48	32.4	2076 ± 21	2075 ± 21	0	2.632	1.2	0.1283	1.2	6.72	1.7	0.3801	1.2	0.695
8.1	0.14	81	32	0.41	27.3	2121 ± 23	2121 ± 26	0	2.561	1.3	0.1317	1.5	7.08	1.9	0.3897	1.3	0.654
9.1	0.00	110	56	0.52	36.6	2102 ± 20	2095 ± 20	0	2.594	1.1	0.1298	1.1	6.9	1.6	0.3856	1.1	0.706
10.1	0.50	50	15	0.32	16.9	2140 ± 28	2137 ± 45	0	2.524	1.5	0.1329	2.6	7.22	3	0.3937	1.6	0.518
11.1	0.34	78	31	0.41	25.7	2086 ± 23	2101 ± 34	1	2.606	1.3	0.1303	1.9	6.86	2.3	0.3821	1.3	0.559
12.1	0.00	102	46	0.47	33.4	2087 ± 21	2085 ± 25	0	2.615	1.2	0.1291	1.4	6.81	1.8	0.3824	1.2	0.637
Sample 896																	
1.1	0.05	183	104	0.58	62.9	2164 ± 31	2112 ± 17	−2	2.505	1.7	0.1310	1.0	7.21	1.9	0.3990	1.7	0.866
2.1	0.15	491	189	0.40	157	2036 ± 28	2031 ± 12	0	2.688	1.6	0.1251	0.7	6.41	1.7	0.3713	1.6	0.926
3.1	0.23	152	97	0.66	45.8	1934 ± 29	2024 ± 27	5	2.850	1.7	0.1247	1.5	6.01	2.3	0.3499	1.7	0.743
4.1	0.40	143	92	0.66	44.1	1966 ± 29	2038 ±26	4	2.790	1.7	0.1257	1.5	6.18	2.3	0.3567	1.7	0.761
5.1	0.61	199	124	0.64	63	2007 ± 30	2029 ± 26	1	2.717	1.7	0.1250	1.5	6.3	2.3	0.3653	1.7	0.762
5.2	0.04	633	167	0.27	192	1945 ± 27	1964 ± 18	1	2.838	1.6	0.1205	1.0	5.85	1.9	0.3522	1.6	0.838
6.1	0.50	116	22	0.20	36.9	2015 ± 30	2038 ± 28	1	2.708	1.8	0.1256	1.6	6.36	2.4	0.3670	1.8	0.743
6.2	0.09	634	134	0.22	197	1985 ± 27	1968 ± 11	−1	2.770	1.6	0.1208	0.6	6.01	2.3	0.3607	1.6	0.933
7.1	0.15	110	91	0.85	34.9	2022 ± 31	2013 ± 29	0	2.710	1.8	0.1239	1.7	6.29	2.4	0.3683	1.8	0.729
8.1	0.26	187	111	0.61	62.8	2116 ± 31	2114 ± 24	0	2.565	1.7	0.1312	1.4	7.03	2.2	0.3886	1.7	0.781
Sample 899																	
1.1	–	839	259	0.32	256	1962 ± 14	1958 ± 17	0	2.811	0.8	0.1201	1.0	5.892	1.3	0.3558	0.8	0.661
1.2	0.08	271	81	0.31	82.9	1963 ± 18	1955 ± 20	0	2.809	1.1	0.1199	1.1	5.886	1.5	0.3559	1.1	0.697
2.1	0.00	445	154	0.36	135	1955 ± 16	1983 ± 15	1	2.823	0.9	0.1218	0.8	5.952	1.3	0.3543	0.9	0.760
2.2	–	301	87	0.30	91.8	1961 ± 15	1991 ± 19	2	2.813	0.9	0.1224	1.0	5.998	1.4	0.3555	0.9	0.656
3.1	0.10	811	281	0.36	248	1963 ± 13	1972 ± 13	0	2.809	0.7	0.1211	0.7	5.942	1.1	0.3559	0.7	0.728
3.2	0.16	325	97	0.31	99.3	1958 ± 15	1992 ± 20	2	2.816	0.9	0.1224	1.1	5.991	1.4	0.355	0.9	0.630
4.1	0.08	658	185	0.29	200	1953 ± 13	1960 ± 14	0	2.826	0.8	0.1203	0.8	5.866	1.1	0.3538	0.8	0.718
4.2	0.14	271	90	0.34	82.2	1948 ± 27	1964 ± 21	1	2.833	1.6	0.1205	1.2	5.87	2.0	0.3529	1.6	0.804
5.1	0.08	374	142	0.39	114	1959 ± 17	1975 ± 18	1	2.816	1.0	0.1213	1.0	5.937	1.4	0.3551	1	0.716
6.1	0.05	729	220	0.31	225	1979 ± 13	1946 ± 13	−2	2.783	0.7	0.1193	0.7	5.912	1.1	0.3593	0.7	0.745
7.1	0.03	982	260	0.27	301	1969 ± 13	1993 ± 17	1	2.799	0.7	0.1225	0.9	6.036	1.2	0.3573	0.7	0.634
8.1	0.04	718	157	0.23	220	1969 ± 13	1975 ± 11	0	2.801	0.7	0.1213	0.6	5.973	1.0	0.3571	0.7	0.779
9.1	0.19	325	138	0.44	98.6	1948 ± 15	1952 ± 17	0	2.834	0.8	0.1197	0.9	5.823	1.3	0.3527	0.8	0.686
10.1	0.05	194	48	0.26	59.1	1957 ± 20	1982 ± 31	1	2.819	1.2	0.1217	1.7	5.95	2.1	0.3547	1.2	0.557
11.1	0.06	585	163	0.29	178	1949 ± 13	1955 ± 15	0	2.833	0.7	0.1199	0.9	5.835	1.2	0.3529	0.7	0.674

Pb_c and Pb* are common and radiogenic lead. Calibration error of standard is 0.36%. (1) correction for ^{204}Pb. D—discordance. (Rho) correlation coefficient. Errors of single analyses (ratios and ages) are given at 1σ level, errors of calculated ages in Figs. 6–8 are given at 2σ level.

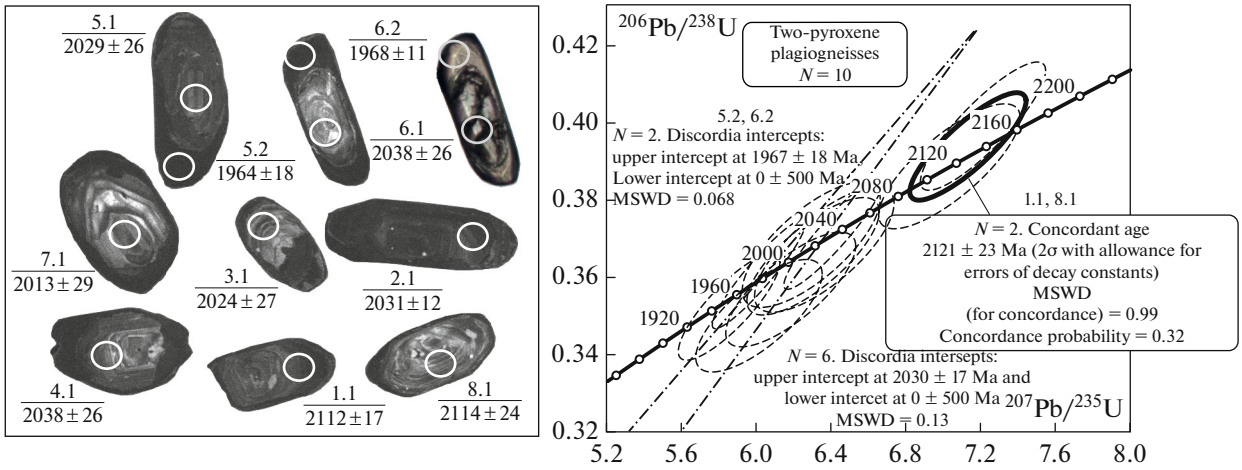

Fig. 7. Cathodoluminescence (CL) images and age of zircon from two-pyroxene plagiogneisses (sample 896). For spots 6.1 and 6.2, optical image is shown to the right.

indicates a very short crustal residence time of the magma source with a minimum contribution of Archean crustal material.

Isotope Lu-Hf composition was studied in zircon in six points (sample 231, Fig. 6, Table 4). In the $^{176}Lu/^{177}Hf$–$^{176}Hf/^{177}Hf$ diagram, the analyses define trend related to the metamorphic alterations (including anatexis). A positive correlation between $^{176}Lu/^{177}Hf$ and $^{176}Hf/^{177}Hf$ (dashed line in Fig. 10a) indicates changes of the zircon in a closed system (Chen et al., 2010). This is a result of changes of primary magmatic zircon, because newly formed zircon has the higher $^{176}Hf/^{177}Hf$ ratio than primary zircon (Gerdes and Zeh, 2009). An increase of $^{176}Hf/^{177}Hf$ ratio during metamorphism and anatexis is caused by the isotope exchange between zircon and mineral/melt, because rock-forming minerals and melt have the higher Lu/Hf ratio and hence, more radiogenic Hf composition (Chen et al., 2010). The lowest ratio $^{176}Lu/^{177}Hf = 0.00071$ was obtained in spot 6.1 with an age of 2105 ± 26 Ma and can be considered as that of primary zircon. The highest $^{176}Lu/^{177}Hf = 0.000203$ was obtained in spot 9.1 with an age of 2095 ± 20 Ma and suggests that this zircon was transformed during metamorphism and partial melting of rocks. The value of $\varepsilon_{Hf}(T)$ is positive and varies from +6.5 to +12 (Table 4). Such values are typical of depleted mantle (Fig. 10b). Only spot 6.1 with minimum value of $^{176}Lu/^{177}Hf = 0.00071$ plots in this line. Other analyses plot above the depleted mantle curve owing to the metamorphic transformations with an increase of $^{176}Lu/^{177}Hf$ ratio. Model zircon age $T_{Hf}(DM) = 1.98–2.22$ Ga practically coincides with crust extraction time of $T_{Hf}^{C} = 1.99–2.28$ Ga, which indicates that zircon did not interact with crustal rocks and can be interpreted as a growth in juvenile rocks of a new crust, a source of which was depleted mantle. Data on zircon xenocrysts from kimberlites in the Khapchan terrane (Kostrovitsky et al., 2016) presented in Fig. 10b show that the oldest Paleoproterozoic zircons with an age of 2.1 Ga in terms of $\varepsilon_{Hf}(T)$ are also close to the depleted mantle evolution curve.

DISCUSSION

The studied granulite sequence is made up of crystalline schists and orthogneisses with subordinate metasedimentary intercalations. According to the widespread point of view, the granulites are dehydrated residue of high-temperature anatexis of rocks in the lower and middle crust. Incongruent melting of hydrous minerals (amphibole, biotite) produces significant volumes of granitoid melts (Harley, 1989), which escape to higher crustal levels. The studied granulites are represented by rocks with metamorphic banding, where partial melts remained practically in situ (Figs. 3a, 3b, 3c, 3f), and diverse migmatites (Figs. 3c, 3e) with clearly expressed melt segregation. The former suggests isochemical transformations of rocks. In the latter case, it is hardly probable to establish the composition of initial rock (Khodorevskaya, 2019; Bushmin et al., 2020). During anatexis of mafic and intermediate igneous rocks, Rb, Ba, as well as conditionally inert elements Nb, Ta, Zr, and Hf are strongly incompatible with granulite residue (Nehring et al., 2010). In addition, the granulite metamorphism and anatexis led to the separation of Nb and Ta, which affects the Nb/Ta ratio (Nehring et al., 2010; Hoffmann et al., 2011). Therefore, the element ratios rather than their absolute values are more reliable for correct geochemical reconstructions (Pearce, 1996).

Determination of granulite protolith. Magmatic or sedimentary origin of granulite protolith was verified on the petrochemical diagram (Fig. 11a) according to (Werner et al., 1987). Most of the rocks are identified

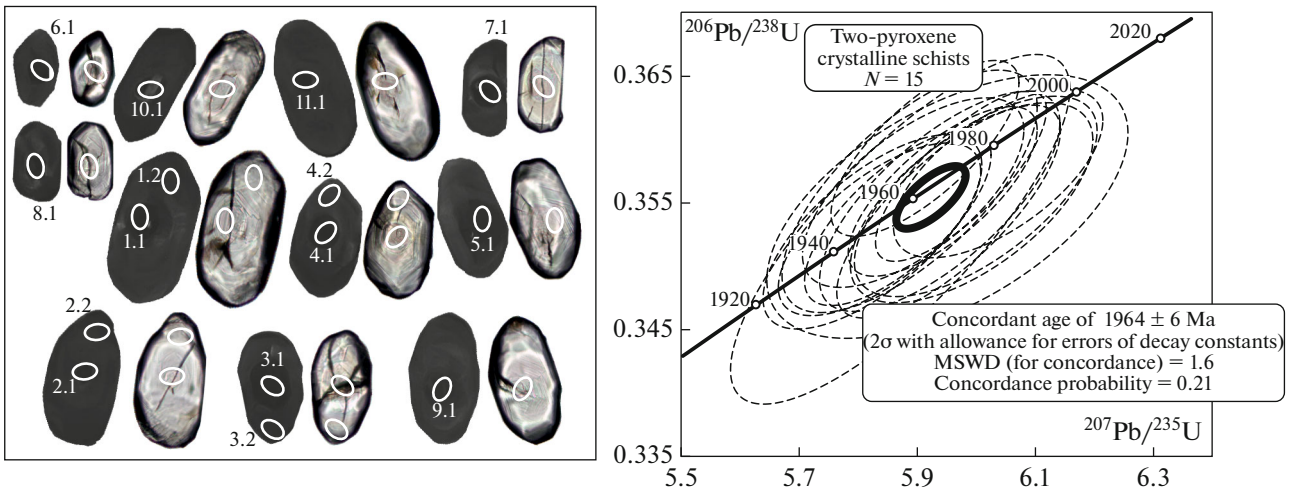

Fig. 8. Cathodoluminescence and optical (paired) images and age of zircon from mafic two-pyroxene crystalline schists (sample 899).

as metamagmatic rocks, while all mafic granulites, two analyses of orthopyroxene gneisses, and garnet gneisses of the Khapchan Group fall in the field of metasedimentary rocks. Sedimentary protolith for the garnet gneisses of the Khapchan Group was confirmed by geological and structural observations (Zlobin et al., 2002) and leaves no doubts.

Chemically, the mafic granulites correspond to mafic rocks (Fig. 4a) and fall in the field of metasedimentary rocks (Fig. 11) owing to their high MgO/CaO ratio. It is noteworthy that dolerites of the unambiguously magmatic Siberian traps in the diagram (Werner et al., 1987) also fall in the field of metasedimentary rocks. This diagram likely has limitations, in particular, cannot be used for high-Mg troctolites and troctolite-dolerites.

Affiliation of protolith of the orthopyroxene granulites (samples 564 and 565A) to metasedimentary rocks is also inferred, because is not confirmed by trace-element indicator ratios. They have low Th/U = 1.4–2.2 (for sedimentary rocks >6 (Nozhkin and Turkina, 1993)), Th/Sc = 0.02–0.03 (Th/Sc = 1–2 for sedimentary rocks (Nozhkin and Turkina, 1993)), and La/Th = 17–28.8 (La/Th = 2.7–3.6 for sedimentary rocks (McLennan et al., 1980)).

There are grounds to suggest that the granulites were formed mainly after volcanoplutonic rocks of wide compositional range from mafic to felsic composition. In terms of alkalinity, the considered rocks are normal and mild-alkaline. The melanocratic and mesocratic granulites are ascribed to the tholeiitic series, while the leucocratic varieties and mafic granulites (sample 899) in Fig. 4c fall in the field of calc-alkaline rocks. However, in the diagram Zr/Y versus Th/Yb (Fig. 11b), all mafic granulites (samples 235, 236, 899), plagioschists (sample 231), and orthopy-

Table 3. Sm and Nd isotope composition of the rocks of the Khapchan site

Sample number	Age, Ma	Sm, ppm	Nd, ppm	$^{147}Sm/^{144}Nd$	$^{143}Nd/^{144}Nd$	$\varepsilon_{Nd}(T)$	$T_{Nd}(DM)$, Ga	$T_{Nd}(DM\text{-}2st)$, Ga
231	2100	6.198	24.970	0.1501	0.512196	4.0	2.28	2.22
235	2100	1.609	5.109	0.1904	0.512767	4.2		
236	2100	1.449	5.045	0.1737	0.512487	3.3		
561	2100	5.604	25.87	0.1310	0.511903	3.4	2.29	2.27
896	2030	2.502	13.971	0.1083	0.511575	2.3	2.27	2.30
897	2100	8.732	36.52	0.1445	0.512084	3.3	2.34	2.28
899	2100	5.204	18.400	0.1710	0.512417	2.6		
900	2100	4.14	20.07	0.1247	0.511820	3.5	2.27	2.26
900-1	2000	1.891	12.87	0.0888	0.511335	2.3	2.21	2.28
49-4	2000	7.729	44.25	0.1056	0.511497	1.1	2.32	2.37

Sample numbers correspond to those of Table 1.

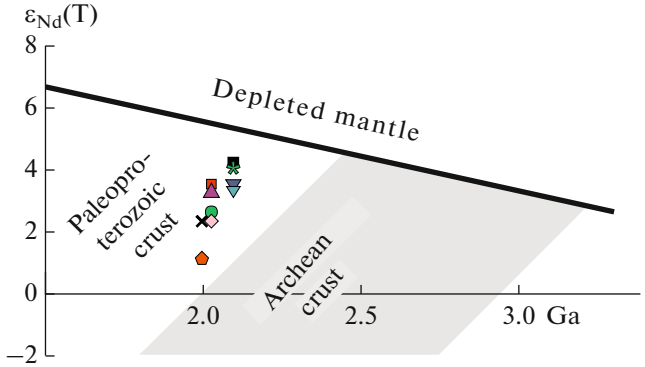

Fig. 9. Diagram $\varepsilon_{Nd}(T)$–age for the rocks of the Khapchan site. Symbols correspond to those in Fig. 4. Evolution curve of Nd isotope composition in a mantle source according to (Goldstein and Jacobsen, 1988).

roxene plagiogneisses (sample 564) are ascribed to the tholeiitic series. Two-pyroxene plagioschists (sample 896) and migmatite leucosome (samples 900, 900-1) are classed with the calc-alkaline rocks. Other rocks are intermediate between the tholeiitic and calc-alkaline series. All rocks have positive $\varepsilon_{Nd}(T)$ from +2.3 to +4.2 and plot closely to the depleted mantle Nd evolution curve, which indicates a short crustal residence time.

Mafic and ultramafic crystalline schists were likely formed after mafic protolith, which was derived from basaltic magma differentiated under crustal conditions based on Eu-minimum in metapyroxenites. It is possible that ultramafic rocks are partially residual rocks, while their Eu minimum is related to the plagioclase fractionation.

Plagioschists and gneisses were likely formed after rocks similar to diorite, tonalite, and trondhjemite or their volcanic analogues. Zircon dating revealed two magmatic episodes, which are confirmed by differences in rock geochemistry. The crystallization age of the diorite protolith of two-pyroxene plagioschists is 2095 ± 10 Ma. Zircon of close age (2121 ± 23 Ma) is present as inherited in the two-pyroxene gneisses of tonalite composition (sample 896). Prevailing zircon with rhythmic (magmatic) zoning in this sample has an age of 2030 ± 17 Ma, which is considered as the crystallization age of tonalite protolith of two-pyroxene gneisses, sample 896.

Thus, the first magmatic episode, which produced the protoliths of two-pyroxene plagioschists and gneisses, was represented by tholeiitic rock series formed 2100 Ma. The isotope Lu-Hf composition of zircon with an age of 2095 ± 10 Ma indicates that its composition corresponded to the depleted mantle reservoir.

The second magmatic episode is marked by zircon with an age of 2030 ± 17 Ma in two-pyroxene plagiogneisses. These rocks differ in the well expressed negative Nb, Ta, Ti, P anomalies typical of subduction settings (Pearce, 1996).

Migmatites. Partial melting of rocks during metamorphism is related to the formation of CL-black zircon within 1967–1964 Ma. Migmatites are widespread at the studied area. Anatexis occurred in two stages and produced, respectively, diatexites and trondhjemites intersecting them (Fig. 3c). The diatexites (sample 900) are the most siliceous among the studied rocks and in composition correspond to trondhjemites, have relatively low $(La/Yb)_N = 5.54$, Sr/Y = 7.5, positive Eu-anomaly (Eu/Eu* = 1.12), and the highest Nb/Ta = 39.7. The high Nb/Ta = 25–40 is typical of the lower crustal melts (Hoffman et al., 2011). The low $(La/Yb)_N$ indicates the absence of garnet in residue and the possible generation of the melt under amphibolite facies conditions.

The trondhjemite leucosome of vein migmatites (sample 900-1) differs in the expressed positive Eu-anomaly (Eu/Eu* = 2.62) and fractionated REE pattern ($(La/Yb)_N = 18.3$). Experimental data on melting of mafic granulites and the positive Eu anomaly indicate a pressure less than 10 kbar (Springer and Seek, 1997). The low (in ppm) Yb 0.87 and Y 6.69 at high Sr 406 point to a significant fraction of garnet and

Table 4. Lu-Hf isotope composition of zircon from mesocratic crystalline schists of sample 231

Analysis spot	T, Ma	$\frac{^{176}Yb}{^{177}Hf}$	$\frac{^{176}Lu}{^{177}Hf}$	$\frac{^{176}Hf}{^{177}Hf}$	±σ	$\varepsilon_{Hf}(T)$	±2σ	$T_{Hf}(DM)$, Ga	T^C_{Hf}, Ga
1	2125	0.03757	0.00162	0.281831	0.000024	12.0	0.13	2.03	1.99
6	2105	0.01644	0.00071	0.281652	0.000024	6.5	0.15	2.22	2.28
7	2075	0.03389	0.00162	0.281868	0.000022	12.2	0.09	1.98	1.93
9	2095	0.03528	0.00203	0.281842	0.000027	11.1	0.26	2.03	2.01
10	2137	0.01968	0.00117	0.281723	0.000034	9.1	0.47	2.15	2.16
11	2101	0.02578	0.00136	0.281788	0.000023	10.3	0.11	2.07	2.06

Position and numbers of measurement spots correspond to those of Fig. 5. (T) $^{207}Pb/^{206}Pb$ zircon age; $T_{Hf}(DM)$—model age; (T^C_{Hf}) crustal extraction time (two-stage age) calculated using the average $^{176}Lu/^{177}Hf = 0.015$ for felsic crust (Griffin et al., 2014).

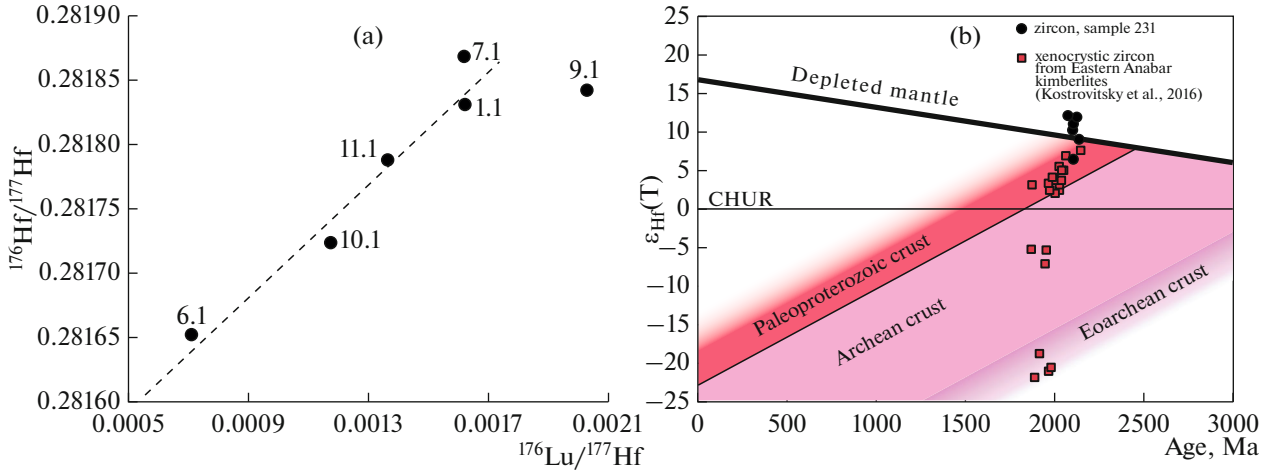

Fig. 10. Diagrams $^{176}Hf/^{177}Hf$–$^{176}Lu/^{177}Hf$ (a) and $\varepsilon_{Hf}(T)$–age (b) for zircons from plagioschists of sample 231. Numerals in the diagrams are analyses shown in Fig. 6 and Table 4. CHUR is the chondrite uniform reservoir. In the diagram (a), dashed line shows a trend of metamorphic alterations of zircon composition.

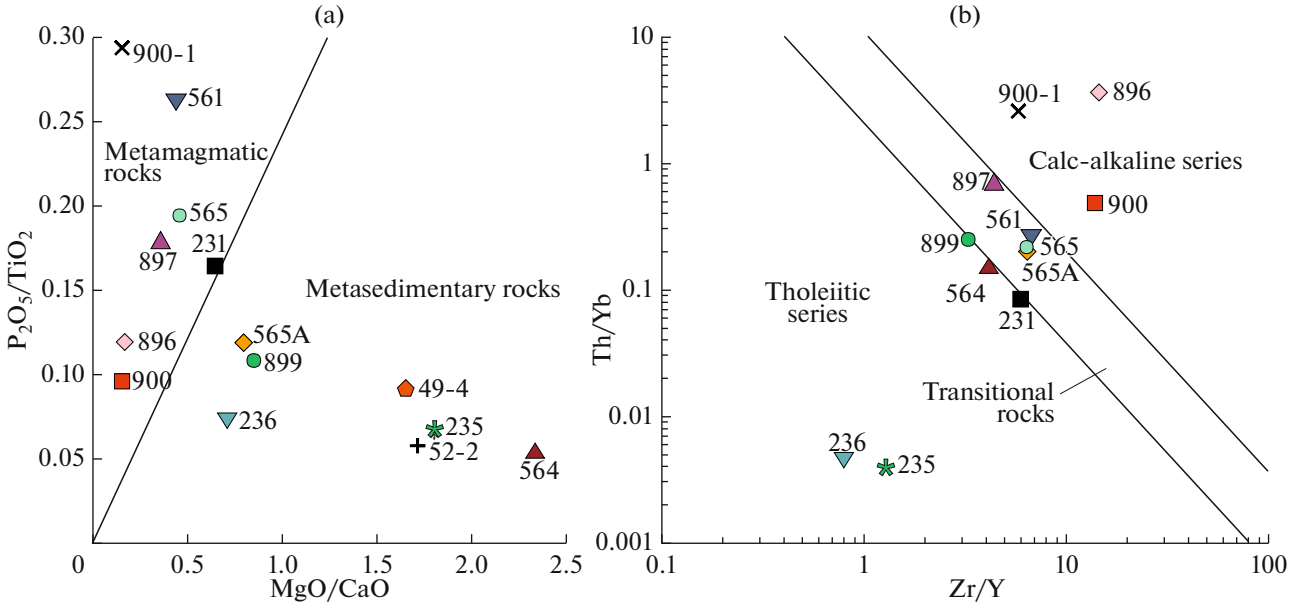

Fig. 11. Diagrams P_2O_5/TiO_2–MgO/CaO after (Werner et al., 1987) (a) and Th/Yb– Zr/Y after (Ross and Bedard, 2009) (b) for granulites of the Khapchan site.

absence of plagioclase in the residue. A depletion in Ta (0.14 ppm) at Nb 2.75 ppm corresponds to Nb/Ta = 19.6, which is typical of migmatitic TTG (tonalite–trondhjemite–granodiorite) series (Nb/Ta = 14–42) formed during partial melting under the granulite facies conditions. (Hoffman et al., 2011). The high $(La/Yb)_N$ = 18.9 and Sr/Y = 60.7 make them similar to the TTG granitoids.

Thus, the geochemical features of migmatites suggest that the diatexites were formed under amphibolite facies conditions, while later vein migmatites, under granulite facies metamorphism.

Possible geodynamic setting of the formation of granulite protoliths. The geodynamic settings of the formation of initial rocks were interpreted using diagrams (Fig. 12) with immobile (HFSE) elements: Ta, Yb, Th, Nb, Ti. Diagrams 12a and 12b could be additionally used for rocks of mafic and felsic composition; Figs. 12c and 12d, for mafic rocks; and Figs. 12e and 12 f, for rocks of felsic composition. In the diagrams (Figs. 12a, 12b), the rock compositions fall in the same fields: the majority of data points fall in the

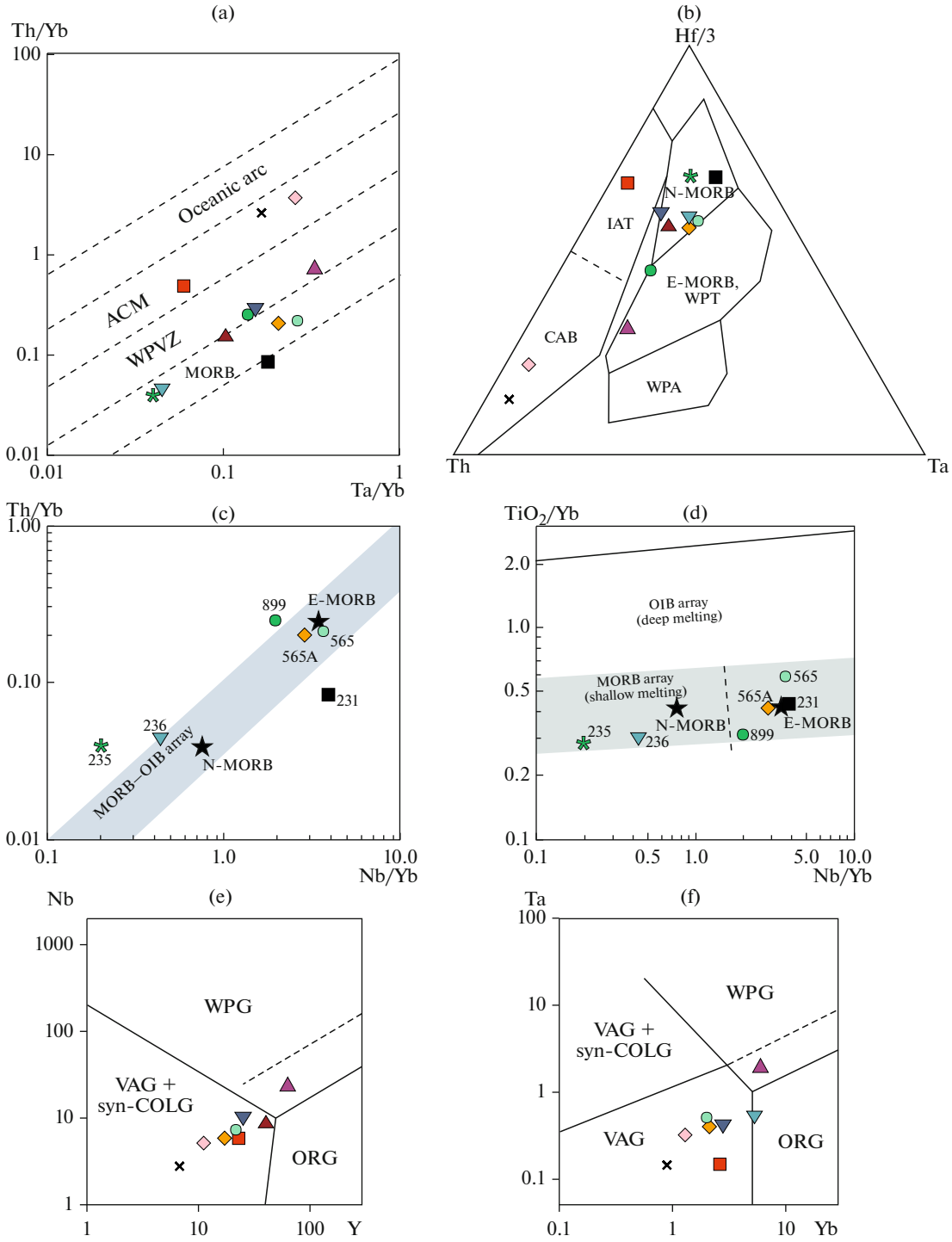

Fig. 12. Geodynamic discrimination diagrams: (a) (Shandl and Gorton, 2002); (b) (Wood, 1980); (c, d) (Pearce, 2008); (e, f) (Pearce, 1984). Data points correspond to those of Fig. 4. Fields in the diagram (a): (ACM) active continental margins, (WPVZ) within-plate volcanic zones, (MORB) mid-ocean ridge basalts. In the diagram (b): (N-MORB) normal mid-ocean ridge basalts, (E-MORB) enriched mid-ocean ridge basalts, (WPT) within-plate tholeiites, (WPA) within-plate alkaline basalts, (IAT) primitive island-arc tholeiites; (CAB) calc-alkaline tholeiites of volcanic arcs. In the diagrams (c), (d) asterisks show the average composition of N-MORB and E-MORB basalts, dashed line shows the boundary between them; numerals of samples of mafic and mesocratic granulites are indicated. Fields in the diagrams (e), (f): (WPG) within-plate granites, (VAG) volcanic-arc granites, (syn-COLG) syn-collisional granites, (ORG) granites of "normal" ocean-ridge, the main volcanic product of which is N-MORB-type basalt. Dashed line represents the upper boundary of compositions for ORG from segments of anomalous ridge, where eruption products are represented by E-MORB or T-MORB, i.e., are enriched in incompatible trace elements.

MORB field in Fig. 12a and in the N-MORB field in Fig. 12b with transition to fields of enriched rocks of within-plate volcanic zones (WPVZ) in Fig. 12a, within-plate tholeiites (WPT) and enriched basalts (E-MORB) in Fig. 12b. Orthopyroxene plagiogneisses (sample 879) enriched in plagioclase (56%) and REE (ΣREE = 184.7 ppm), with deep Eu minimum (Eu/Eu* = 0.46) fall beyond the N-MORB field. Two-pyroxene gneisses with an age of 2030±17 Ma (sample 869), diatexites (sample 900), and migmatite leucosome (sample 900-1) are clustered separately in fields related to subduction magmatism (ACM, CAB, IAT) in (Figs. 12a, 12b).

Granulites corresponding in composition to mafic and intermediate rocks in Fig. 12c follow MORB–OIB array. Ultramafic and mafic crystalline schists (samples 235, 236) fall in the vicinity of the average N-MORB, while other compositions are restricted to the average enriched E-MORB-type basalt. Crustally contaminated rocks (samples 235 and 899) are plotted above this trend (Pearce, 2008), which is determined by their elevated Th content. Analysis of sample 212 falls below MORB–OIB trend, which is related to the low content of Th = 0.27 ppm. However, this sample in Fig. 12d falls practically in the point of average E-MORB. In addition, zircon from this sample with an age of 2095 ± 10 Ma has $\varepsilon_{Hf}(T)$ typical of depleted mantle (Table 4). It is suggested that mafic protoliths were formed through melting at shallow depth.

It is suggested that subduction in the northeastern Siberian Platform played a decisive role in the diamond formation, because placers of the northeastern Yakutian Province contain mainly eclogitic diamonds (Sun et al., 2020; Shatsky et al., 2016; Zedgenizov et al., 2016). A reconstructed composition of an eclogite with positive Eu and Sr anomalies suggests that the protolith for eclogitic diamond was subducted rocks of oceanic crust (Shatsky et al., 2016). It is believed that the eclogites of the Obnazhennaya pipe in the Birekta terrane represent a gabbroid part of subducted or subsided basaltic crust, which was subjected to long-term high-pressure partial melting with residual garnet (Sun et al., 2020). The formation of eclogites was related to the high-pressure metamorphism, which theoretically is reached in subduction zones during rock subsidence at a depth of 60 km corresponding to a pressure of ca. 2 GPa.

Our data confirm the existence of juvenile crust with an age of 2.1 Ga and subduction processes with an age of 2030 ± 17 Ma, which likely were responsible for the eclogite formation. Obtained Lu-Hf isotope data on zircon from sample 231 are comparable with those of Paleoproterozoic zircon xenocrysts from kimberlites in the Khapchan terrane, which indicates a depleted mantle reservoir (Kostrovitsky et al., 2016). Compared to the >2 Ga Paleoproterozoic xenocrysts from kimberlites ($\varepsilon_{Hf}(T)$ = 2.0–7.6, $T_{Hf}(DM)$ = 2.16–2.32 Ga), the studied zircons have slightly higher $\varepsilon_{Hf}(T)$ values, while model ages of $T_{Hf}(DM)$ and T^{C}_{Hf} are slightly lower (Table 4), which is related to a change of zircon isotope composition (Fig. 10a) during metamorphism and anatexis.

The formation of the juvenile crust in the Paleoproterozoic in the Birekta terrane is related to the mantle processes in the central part of the Siberian Craton (Ionov et al., 2015; Shatsky et al., 2018, 2019). Based on Re-Os dating of peridotite xenoliths from kimberlites of the Udachnaya Pipe, the main episode of the formation of lithospheric mantle in the central part of the craton (Daldyn terrane) and, likely, in its southern and southeastern parts (Mir pipe) also occurred in the Paleoproterozoic 2.1 Ga (Ionov et al., 2015).

CONCLUSIONS

The granulite complex in the Khapchan River mouth is made up of metamagmatic rocks widely varying from mafic to felsic compositions. These rocks have positive Nd isotope values $\varepsilon_{Nd}(T)$ from +2.3 to +4.2, which indicates the contribution of mantle source in magma formation. Mafic granulites are ascribed to the tholeiitic series and have N-MORB geochemical signatures. The Lu-Hf systematics of zircon with an age of 2095 ± 10 Ma indicates a depleted mantle reservoir and, as a result, the existence of juvenile crust of this age. The geochemical features of the granulites suggest that the juvenile crust was represented by N-MORB and E-MORB basalts. The granulites with a protolith age of 2030 ± 17 Ma geochemically affiliate with calc-alkaline subduction-related granitoids. Metamagmatic rocks of the Khapchan terrane are interpreted as metamorphosed juvenile suprasubduction complex.

Subduction of oceanic crust of this age could be responsible for the formation of eclogitic assemblage in diamonds, which is widespread in the placer deposits of the northeastern Siberian Platform.

ACKNOWLEDGMENTS

We are grateful to reviewers for constructive comments, which significantly improved this paper.

FUNDING

This study was financially supported by the Russian Foundation for Basic Research (project no. 18-35-00229/18 mol_a) and made in the framework of the State Task of the Institute of Precambrian Geology and Geochronology (project no. 0153-2019-0002).

REFERENCES

Black, L.P., Kamo, S.L., Allen, C.M., et al., TEMORA 1: a new zircon standard for Phanerozoic U-Pb geochronology, *Chem. Geol.,* 2003, vol. 200, pp. 155–170.

Blichert-Toft, J. and Albarede, F., The Lu-Hf isotope geochemistry of chondrites and evolution of the crust–mantle system, *Earth Planet. Sci. Lett.,* 1997, vol. 148, pp. 243–258.

Bushmin, S.A., Vapnik, E.A., Ivanov, M.V., et al., Fluids in high-pressure granulites, *Petrology,* 2020, vol. 28, no. 1, pp. 17–46.

Chauvel, C. and Blichert-Toft, J., A hafnium isotope and trace element perspective on melting of the depleted mantle, *Earth Planet. Sci. Lett.,* 2001, vol. 190, pp. 137–151.

Chen, R.-X., Zheng, Y.-F., and Zie, L., Metamorphic growth and recrystallization of zircon: distinction by simultaneous in-situ analyses of trace elements. U-Th-Pb and Lu-Hf isotopes in zircon from eclogite-facies rocks in the Sulu Orogen, *Lithos,* 2010, vol. 114, pp. 132–154.

Condie, K.C., Wilks, M., Rosen, O.M., and Zlobin, V.L., Geochemistry of metasediments from the Precambrian Hapschan Series, eastern Anabar Shield, Siberia, *Precambrian Res.,* 1991, vol. 50, pp. 37–47.

O'Connor, J.T., A classification for quartz-rich igneous rocks based on feldspar ratios, *US Geol. Surv. Prof. Pap.,* 1965, pp. 79–84.

Elhlou, S., Belousova, E., Griffin, W.L., et al., Trace element and isotopic composition of gj red zircon standard by laser ablation, *Geochim. Cosmochim. Acta,* 2006, vol. 70, p. A158.

Gerdes, A. and Zeh, A., Zircon formation versus zircon alteration - new insights from combined U-Pb and Lu-Hf in-situ LA-ICP-MS analyses, and consequences for the interpretation of Archean zircon from the central zone of the Limpopo Belt, *Chem. Geol.,* 2009, vol. 261, pp. 230–243.

Goldstein, S.J. and Jacobsen, S.B., Nd and Sm isotopic systematics of river water suspended material: implications for crustal evolution, *Earth Planet. Sci. Lett.,* 1988, vol. 87, pp. 249–265.

Griffin, W.L., Ryan, C.G., Kaminsky, F.V., et al., The Siberian lithosphere traverse, mantle terranes and the assemble of the Siberian Craton, *Tectonophysics,* 1999, vol. 310, pp. 1–35.

Griffin, W.L., Pearson, N.J., Belousova, E., et al., The Hf isotope composition of cratonic mantle: LAM-MC-ICP-MS analysis of zircon megacrysts in kimberlites, *Geochim. Cosmochim. Acta,* 2000, vol. 64, pp. 133–147.

Griffin, W.L., Belousova, E.A., O'Neill, C., et al., The world turns over: Hadean–Archean crust–mantle evolution, *Lithos,* 2014, vol. 189, pp. 2–15.

Harley, S.L., The origins of granulites: a metamorphic perspective, *Geol. Mag.,* 1989, vol. 126, pp. 215–247.

Hastie, A.R., Kerr, A.C., Pearce, J.A., and Mitchell, S.F., Classification of altered volcanic island arc rocks using immobile trace elements: development of the Th-Co discrimination diagram, *J. Petrol.,* 2007, vol. 48, pp. 2341–2357.

Hoffmann, J.E. Münker, C., Næraat, T., et al. Mechanisms of Archean crust formation inferred from high-precision HFSE systematics in TTGs, *Geochim. Cosmochim. Acta,* 2011, vol. 75, pp. 4157–4178.

Ionov, D.A., Doucet, L.S., Carlson, R.W., et al., Post-Archean formation of the lithospheric mantle in the central Siberian Craton: Re-Os and PGE study of peridotite xenoliths from the Udachnaya kimberlite, *Geochim. Cosmochim. Acta,* 2015, vol. 165, pp. 466–483.

Izotopnaya geologiya noril'skikh mestorozhdenii (Isotope Geology of the Norilsk Deposits), St. Petersburg: Izd. VSEGEI, 2017.

Jacobsen, S.B. and Wasserburg, G.J., Sm-Nd evolution of chondrites and achondrites, *Earth Planet. Sci. Lett.,* 1984, vol. 67, pp. 137–150.

Kapitonov I.N., Adamskaya E.V., Lokhov K.I., Sergeev S.A., Opportunities of LA-ICP-MS technique of $^{176}Hf/^{177}Hf$ determination in the oldest (>3 Ga) zircons, *XVIII simpozium po geokhimii izotopov. Tez. dokl.* (Proc. 18th Symposium on Isotope Geochemistry), Moscow: GEOKhI RAN, 2007. C. 117.

Kargin, A.V., Golubeva, Yu.Yu., Demonterova, E.I., and Koval'chuk, E.V., Petrographic-geochemical types of Triassic alkaline ultramafic rocks in the northern Anabar Province, Yakutia, Russia, *Petrology,* 2017, vol. 25, no. 6, pp. 535–565.

Khodorevskaya, L.I., Granitization and high-temperature metasomatism in mafic rocks: comparison between experimental data and natural observations, *Petrology,* 2019, vol. 27, no. 5, pp. 516–533.

Kostrovitsky, S.I., Skuzovatov, S.Y., Yakovlev, D.A., Sun, J., et al., Age of the Siberian Craton crust beneath the northern kimberlite fields: insights to the craton evolution, *Gondwana Res.,* 2016, vol. 39, pp. 365–385.

Lopatin, B.G., and Tabunov, S.M. *Geologicheskaya karta SSSR masshtaba 1 : 200 000. Seriya Anabarskaya. List R-49-XXIII, XXIV. Ob"yasnitel'na zapiska* (Geological Map of the USSR on a Scale 1 : 200 000. Anabar Series. Sheet R-49-XXIII, XXIV. Explanatory Note), Moscow: Nedra, 1969.

Ludwig, K.R., *User's manual for Isoplot/Ex. Version 2.10. A geochronological toolkit for Microsoft Excel*, *Berkeley. Geochronol. Center Spec. Publ.*, 1999, vol. 1.

Ludwig, K.R., *Squid 1.00. A user's manual*, *Berkeley Geochronol. Center Spec. Publ.,* 2000, vol. 2.

Lutts, B.G. and Oksman, V.S., *Glubokoerodirovannye zony razlomov Anabarskogo shchita* (Deeply Eroded Fault Zones of the Anabar Shield), Moscow: Nauka, 1990.

McLennan, S.M., Nance, W.B., and Taylor, S.R., Rare earth element–thorium correlations in sedimentary rocks, and the composition of the continental crust, *Geochim. Cosmochim. Acta,* 1980, vol. 44, pp. 1833–1839.

Nehring, F., Foley, S.F., and Holtta, P., Trace element partitioning in the granulite facies, *Contrib. Mineral. Petrol.,* 2010, vol. 159, no. 4, pp. 493–519.

Nozhkin A.D. and Turkina, O.M., *Geokhimiya granulitov kanskogo i sharyzhalgaiskogo kompleksov* (Geochemistry of Granulites of the Kan and Sharyzhalgai Complexes), Novosibirsk: OIGGM SO RAN, 1993.

Pearce, J.A., Harris, N.W., and Tindle, A.G., Trace element discrimination diagrams for the tectonic interpretation of granitic rocks, *J. Petrol.,* 1984, vol. 25, pp. 956–983.

Pearce, J.A., *A user's guide to basalt discrimination diagrams, Trace Element Geochemistry of Volcanic Rocks: Applications for Massive Sulphide Exploration*. Wyman, D.A., Eds., *Geol. Ass. Can. Short Course Notes*, 1996, vol. 12, pp. 79–113.

Pearce, J.A., Geochemical fingerprinting of oceanic basalts with applications to ophiolite classification and the search for Archean oceanic crust, *Lithos,* 2008, vol. 100, pp. 14–48.

De la Roche, H., Leterrier, J., Grandclaude, P., et al., A classification of volcanic and plutonic rocks using R1–R2

diagram and major element analyses—its relationships with current nomenclature, *Chem. Geol.,* 1980, vol. 29, pp. 183–210.

Rosen, O.M. and Turkina, O.M., *The oldest rock assemblages of the Siberian Craton, Earth's Oldest Rocks, Van Kranendonk, M.J.*, Smithies, R.H., and Bennet, V.C., Eds, *Developments in Precambrian Geology,* 2007, vol. 15, pp. 793–838.

Rosen, O.M., Condie, K.C., Natapov, L.M., and Nozhkin, A.D., *Archean and Early Proterozoic evolution of the Siberian Craton: a preliminary assessment, Archean Crustal Evolution, Condie, K.*, Amsterdam: Elsevier, 1994, pp. 411–459.

Rosen, O.M., Manakov, A.V., and Serenko, V.P., Paleoproterozoic collisiona system and diamondiferous llithospheric keel of the Yakutian kimbelite province, *Russ. Geol. Geophys.,* 2005, vol. 46, no. 12, pp. 1237–1251.

Rosen, O.M., Levsky, L.K., Zhuravlev, D.Z.,et al., Paleoproterozoic accretion in the northeast Siberian Craton: isotopic dating of the Anabar collision system, *Stratigraphy. Geol. Correlation,* 2006, vol. 14, no. 6, pp. 581–601.

Ross, P.-S. and Bedard, J.H., Magmatic affinity of modern and ancient subalkaline volcanic rocks determined from trace-element discriminant diagrams, *Can. J. Earth Sci.,* 2009, vol. 46, pp. 823–839.

Sawyer, E.W., *Atlas of Migmatites, The Canad. Mineral. Spec. Publ.,* 2008, vol. 9.

Schandl, E.S. and Gorton, M.P., Application of high field strength elements to discriminate tectonic settings in VMS environments, *Econ. Geol.,* 2002, vol. 97, pp. 629–642.

Scherer, E., Munker, C., and Mezger, K., Calibration of the lutetium–hafnium clock, *Science,* 2001, vol. 293, pp. 683–687.

Shatsky, V.S., Zedgenizov, D.A., and Ragozin, A.L., Evidence for a subduction component in the diamond-bearing mantle of the Siberian craton, *Russ. Geol. Geophys.,* 2016, vol. 57, no. 1, pp. 111–126.

Shatsky, V.S., Malkovets, V.G., Belousova, E.A., et al., Multi-stage modification of Paleoarchean crust beneath the Anabar tectonic province (Siberian craton), *Precambrian Res.,* 2018, vol. 305, pp. 125–144.

Shatsky, V.S., Wang, Q., Skuzovatov, S.Yu., and Ragozin, A.L., The crust-mantle evolution of the Anabar tectonic province in the Siberian craton: coupled or decoupled?, *Precambrian Res.*, 2019, vol. 332, 105388.

Smelov, A.P., Kotov, A.B., Sal'nikova, E.B., et al., Age and duration of the formation of the Billyakh tectonic melange zone, Anabar Shield, *Petrology,* 2012, vol. 20, no. 3, pp. 286–300.

Springer, W. and Seek, H.A., Partial fusion of basic granulites at 5 to 15 kbar: implications for the origin of TTG magmas, *Contrib. Mineral. Petrol.,* 1997, vol. 127, pp. 30–45.

Sun, S. and McDonough, W.F., Chemical and isotopic systematics of oceanic basalts: implications for mantle composition and processes, *Geol. Soc. Spec. Publ.,* 1989, vol. 42, pp. 313–345.

Sun, J., Rudnick, R.L., Kostrovitsky, S., et al., The origin of low-MgO eclogite xenoliths from obnazhennaya kimberlite, Siberian craton, *Contrib. Mineral. Petrol.,* 2020, vol. 175, p. 25.

Werner, C.D., Saxonian granulites—a contribution to the geochemical diagnosis of original rocks in high-metamorphic complexes, *Gerlands Beitr. Geopys,* 1987, vol. 96, pp. 271–290.

Whitney, D.L. and Evans, B.W., Abbreviations for names of rock-forming minerals, *Am. Mineral.,* 2010, vol. 95, pp. 185–187.

Williams, I.S., U-Th-Pb geochronology by ion-microprobe, *Rev. Econ. Geol.,* 1998, vol. 7, pp. 1–35.

Wood, D.A., The application of a Th-Hf-Ta diagram to problems of tectonomagmatic classification and to establishing the nature of crustal contamination of basaltic lavas of the british tertiary volcanic province, *Earth Planet. Sci. Lett.,* 1980, vol. 50, pp. 11–30.

Woodhead, J., Hergt, J., Shelley, M., et al., Zircon Hf-isotope analysis with an excimer laser, depth profiling, ablation of complex geometries, and concomitant age estimation, *Chem. Geol.,* 2004, vol. 209, pp. 121–135.

Zedgenizov, D.A., Rubatto, D., Shatsky, V.S., et al., Eclogitic diamonds from variable crustal protoliths in the northeastern Siberian Craton: trace elements and coupled δ13C-δ18O signatures in diamonds and garnet inclusions, *Chem. Geol.,* 2016, vol. 422, pp. 46–59.

Zlobin, V.L., Rosen, O.M., and Abbyasov, A.A., Two metasedimentary basins of the Early Precambrian granulites of the Anabar Shield (Polar Siberia): normative mineral compositions calculated by the minlith program and basin facies interpretations, *Precambrian Sedimentary Environments: a Modern Approach to Ancient Depositional Systems,* Blum, M., Ed., International Association of Sedimentologists. Spec. Publ. **33**, pp. 275–291 (2009).

Translated by M. Bogina